

ARTICLE

DOI: 10.1038/s41467-017-01950-1

OPEN

Opposite effects of Activin type 2 receptor ligands on cardiomyocyte proliferation during development and repair

Deepika Dogra¹, Suchit Ahuja¹, Hyun-Taek Kim¹, S. Javad Rasouli¹, Didier Y.R. Stainier^{1,2} & Sven Reischauer^{1,2}

Zebrafish regenerate damaged myocardial tissue very effectively. Hence, insights into the molecular networks underlying zebrafish heart regeneration might help develop alternative strategies to restore human cardiac performance. While TGF- β signaling has been implicated in zebrafish cardiac regeneration, the role of its individual ligands remains unclear. Here, we report the opposing expression response during zebrafish heart regeneration of two genes, *mstnb* and *inhbaa*, which encode TGF- β family ligands. Using gain-of-function (GOF) and loss-of-function (LOF) approaches, we show that these ligands mediate inverse effects on cardiac regeneration and specifically on cardiomyocyte (CM) proliferation. Notably, we find that *Inhbaa* functions as a CM mitogen and that its overexpression leads to accelerated cardiac recovery and scar clearance after injury. In contrast, *mstnb* GOF and *inhbaa* LOF both lead to unresolved scarring after cardiac injury. We further show that *Mstnb* and *Inhbaa* inversely control Smad2 and Smad3 transcription factor activities through alternate Activin type 2 receptors.

¹Department of Developmental Genetics, Max Planck Institute for Heart and Lung Research, 61231 Bad Nauheim, Germany. ²Department of Biochemistry and Biophysics, University of California San Francisco, San Francisco, 94158 CA, USA. Correspondence and requests for materials should be addressed to S.R. (email: sven.reischauer@mpi-bn.mpg.de)

The adult mammalian heart is incompetent to regenerate damaged muscle tissue post myocardial infarction (MI). Instead, lost myocardium is replaced by a functionally and electrically inert fibrotic scar, resulting in compromised cardiac performance and arrhythmia¹. As a consequence, MI is a leading cause of death and morbidity worldwide². Several active fields of research are trying to address this problem by developing various regenerative approaches focusing on the engraftment of stem cell-derived CMs into injured hearts³, the stimulation of CM proliferation in situ⁴, or the in situ trans-differentiation of fibroblasts into functional CMs⁵.

In contrast to mammals, several other vertebrates, including zebrafish, can regenerate injured or lost myocardial tissue⁶ after multiple types of injury, including ventricular resection⁶, cryoinjury⁷, or genetic CM ablation⁸. Consequently, zebrafish serve as an established model to investigate the process of cardiac regeneration. Lineage tracing experiments have reported that remaining CMs in the vicinity of the injured area undergo dedifferentiation and proliferation to give rise to new CMs that subsequently integrate and functionally couple to the remaining myocardium^{9, 10}. Hence, an in-depth understanding of the cellular and molecular processes controlling cardiac

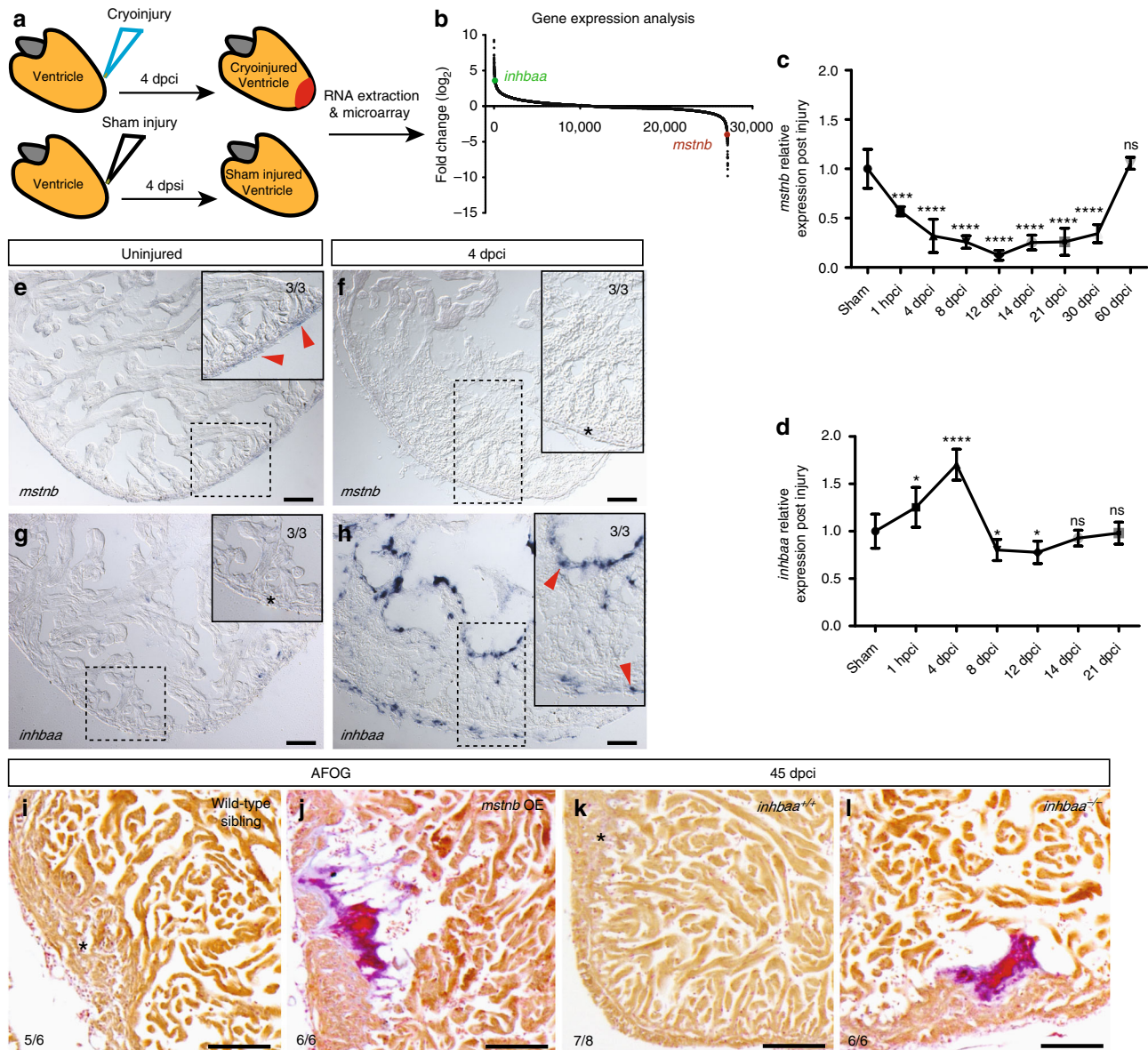


Fig. 1 *mstnb* and *inhbaa* have opposing response and functions during zebrafish cardiac regeneration. **a** Schematic representation of injury and sample preparation for microarray analysis ($n = 12$ hearts). **b** Averaged transcriptional gene expression changes post cryoinjury as assessed by microarray analysis (*inhbaa* and *mstnb* indicated). **c, d** Temporal RT-qPCR analysis for *mstnb* and *inhbaa* expression post cryoinjury ($n = 2 \times 3$ cardiac ventricles assessed as two biological and two technical replicates for each time point, data are mean \pm s.e.m., ns: no significant changes observed, $*P \leq 0.05$, $***P \leq 0.001$, and $****P \leq 0.0001$ —Student's t test, two-tailed). **e-h** In situ hybridization for *mstnb* and *inhbaa* expression on uninjured and 4 dpci adult zebrafish heart sections. Higher magnifications of dashed boxes in **e-h** are shown in upper right corners. RNA probe signal is indicated by red arrowheads and the absence of signal is indicated by asterisks. The numerators indicate the number of hearts with a particular pattern of signal, and the denominators the total number of hearts analyzed. **i-l** AFOG staining of sections from wild-type sibling, *mstnb* OE, *inhbaa*^{+/+}, and *inhbaa*^{-/-} cryoinjured hearts at 45 dpci. Healthy myocardium in orange, fibrin in red, collagen in blue. Asterisks indicate the regions of resolved scarring. The numerators indicate the number of hearts with a particular pattern of scarring, and the denominators the total number of hearts analyzed. Scale bars: in situ hybridization images, 50 μ m; AFOG staining images, 100 μ m.

regeneration appears instrumental to develop alternative therapeutic strategies.

Various signaling pathways including epidermal growth factor (EGF), bone morphogenetic protein, vascular endothelial growth factor, interleukin 6 class cytokines and others have been implicated in the process of cardiac regeneration^{11–13}. Importantly, only Neuregulins (Nrg) and their co-receptor ERBB2 have so far been reported to possess mitogenic activity on CMs, not only after injury, but also on the healthy myocardium of fish and mice^{4, 14–17}. Consequently, Nrg is subject to ongoing research to evaluate its therapeutic potential¹⁸. Members of the transforming growth factor beta (TGF- β) signaling pathway have been implicated in various developmental¹⁹ and disease conditions²⁰, but the role of its numerous components in cardiac regeneration is poorly understood. The vertebrate TGF- β /Activin subfamily (TGF- β family) of ligands is comprised of Activins (INHBA, INHBB), GDFs (Myostatin/GDF8, GDF11) and TGF- β (TGFB1, TGFB2, and TGFB3) which bind Activin type 2 receptors (ACVR2A, ACVR2B, TGFBR2), leading to the recruitment and activation of Activin type 1 receptors (ACVR1B, TGFBR1, ACVR1C). Canonically, this process is followed by phosphorylation of the signal transducers Smad2/3, which bind to Smad4 and translocate to the nucleus, thereby modulating the expression of target genes^{21–23}. Several non-canonical TGF- β pathways have also been reported, which involve mitogen-activated protein kinases (MAPK) and phosphatidylinositol-3-kinase/Akt²⁴. In the diseased mammalian heart, enhanced TGF- β signaling through upregulation of Myostatin (MSTN)²⁵, Inhibin betaA (INHBA)²⁶, and TGF- β ²⁷, stimulates hypertrophy, fibrosis, apoptosis, and endothelial–mesenchymal transition^{28, 29}. Moreover, global myocardial inhibition of TGF- β signaling through CM-specific *Tgfb2* deletion reduces pathological remodeling in response to sustained pressure overload³⁰. In zebrafish, TGF- β signaling is essential for heart regeneration as chemical inhibition of Activin type 1 receptors suppresses CM proliferation and compromises overall cardiac regeneration³¹. MSTN, a well-known negative regulator of skeletal muscle growth^{32, 33}, has been implicated in the development of cardiac hypertrophy in mammals^{34, 35}. Further, the absence of MSTN enhances murine skeletal muscle regeneration³⁶, and a recently developed monoclonal antibody against MSTN shows therapeutic potential in the treatment of skeletal muscle atrophy³⁷. *inhba*, also known as *activin betaA*, promotes wound closure by regulating c-Jun phosphorylation and blastema proliferation during zebrafish fin regeneration³⁸. In sum, the role of TGF- β signaling and its various ligands during heart regeneration and pathology remains unclear. Using gene expression profiling, we identified the opposing expression response of *mstnb* and *inhbaa* to cardiac cryoinjury, calling for a detailed investigation of their specific roles during cardiac regeneration.

Here we show that these two TGF- β family ligands antagonize one another during zebrafish cardiac regeneration. While *mstnb* is robustly and continuously downregulated after cryoinjury in the adult zebrafish heart, *inhbaa* is upregulated. Loss of *mstnb* function and activation of *inhbaa* expression are both beneficial for CM proliferation and lead to enhanced cardiac regeneration. Notably, the overexpression (OE) of *inhbaa* alone is sufficient to induce CM proliferation independently of the well-known Nrg–ErbB signaling pathway. Furthermore, we show that *Mstnb* and *Inhbaa* function through alternate receptor complexes to control the activities of the signal transducers, Smad2 and Smad3, and regulate CM proliferation during development.

Results

***mstnb* and *inhbaa* expression show opposing response to injury.** In order to identify genes differentially regulated during

adult zebrafish heart regeneration, we performed microarray-based expression profiling of whole hearts 4 days post sham injury (dpsi) vs. 4 days post cryoinjury (dpci) (Fig. 1a). Interestingly, we detected opposing expression response of two genes, *mstnb* and *inhbaa*, encoding TGF- β family ligands (Fig. 1b; raw data have been deposited in the NCBI-Gene Expression Omnibus Website—GSE89259). To obtain more detailed temporal expression data, we quantified *mstnb* and *inhbaa* expression in sham and cryoinjured ventricles at different time points post injury using real-time quantitative PCR (RT-qPCR). Consistent with our microarray data, we observed a rapid reduction of *mstnb* transcript levels in regenerating ventricles compared to sham injury, as early as 1 h post cryoinjury (hpci) (Fig. 1c). Interestingly, *mstnb* expression did not return to basal levels before 60 dpci (Fig. 1c), when regeneration was completed⁷, suggesting that a continuous reduction of *mstnb* expression is important for cardiac regeneration. On the contrary, *inhbaa* showed rapid upregulation, peaking at 4 dpci (Fig. 1d); however, by 8 dpci *inhbaa* expression had returned to sham levels (Fig. 1d), indicating a principal role for *inhbaa* during the early phase of cardiac regeneration. To complement the temporal expression data, we analyzed the spatio-temporal pattern of *mstnb* and *inhbaa* expression by in situ hybridization on sections. Interestingly, *mstnb* expression was strongest in the ventricular wall of uninjured hearts (Fig. 1e), and it was reduced below detection levels in 4 dpci samples (Fig. 1f). We also quantified *mstnb* expression levels in uninjured adult hearts by RT-qPCR on laser micro dissected (LMD) tissues and observed higher levels in the ventricular wall over trabecular tissues (Supplementary Fig. 1a). In contrast, no expression of *inhbaa* could be detected in uninjured hearts (Fig. 1g), while it was prominent proximal to the injury site at 4 dpci (Fig. 1h), consistent with published data based on RNA tomography¹¹. To complete our assessment, we examined other TGF- β /Activin ligands and their receptors (refer to Supplementary Table 1 for gene names). Even at a later time point (6 dpci), *inhbaa* and its paralogs *inhbb* and *tgfb3* are the only significantly induced TGF- β family ligand encoding genes, with *inhbaa* showing the most robust upregulation (Supplementary Fig. 1b, c). Taken together, the expression patterns of *inhbaa* and *mstnb* clearly show different spatio-temporal changes during cardiac regeneration.

***mstnb* GOF and *inhbaa* LOF lead to unresolved scarring.** Following our observation that the expression of *mstnb* decreases during cardiac regeneration, we wanted to analyze the effect of sustained *mstnb* expression in regenerating hearts. Hence, we generated a transgenic zebrafish line for CM-specific constitutive OE of *mstnb*, *Tg(myl7:mstnb-2A-H2B-EGFP)* (*mstnb* OE hereafter) (Supplementary Fig. 1d–f). As assessed by RT-qPCR, *mstnb* transcript levels are highly increased in our transgenic *mstnb* OE line compared to non-transgenic siblings (Supplementary Fig. 1g). The gross morphology of adult *mstnb* OE fish and the morphology of their hearts however appear unaffected (Supplementary Fig. 1h–k), indicating that cardiac-specific *mstnb* OE does not affect the development or growth of the zebrafish heart, unlike in mouse hearts, where its OE is reported to cause interstitial fibrosis with compromised cardiac output³⁹.

Next, to determine the role of *inhbaa* during cardiac regeneration, we generated a mutant allele using transcription activator-like effector nuclease (TALEN)-induced mutagenesis. A TALEN targeting the TGF- β propeptide domain was designed (Supplementary Fig. 1l) and a 17 bp deletion allele, *inhbaa*^{bns37} (Supplementary Fig. 1m), which is predicted to encode a truncated protein (Supplementary Fig. 1n) was recovered. In addition, *inhbaa* transcript levels were found to be significantly reduced in *inhbaa*^{-/-} compared to *inhbaa*^{+/+} siblings as shown

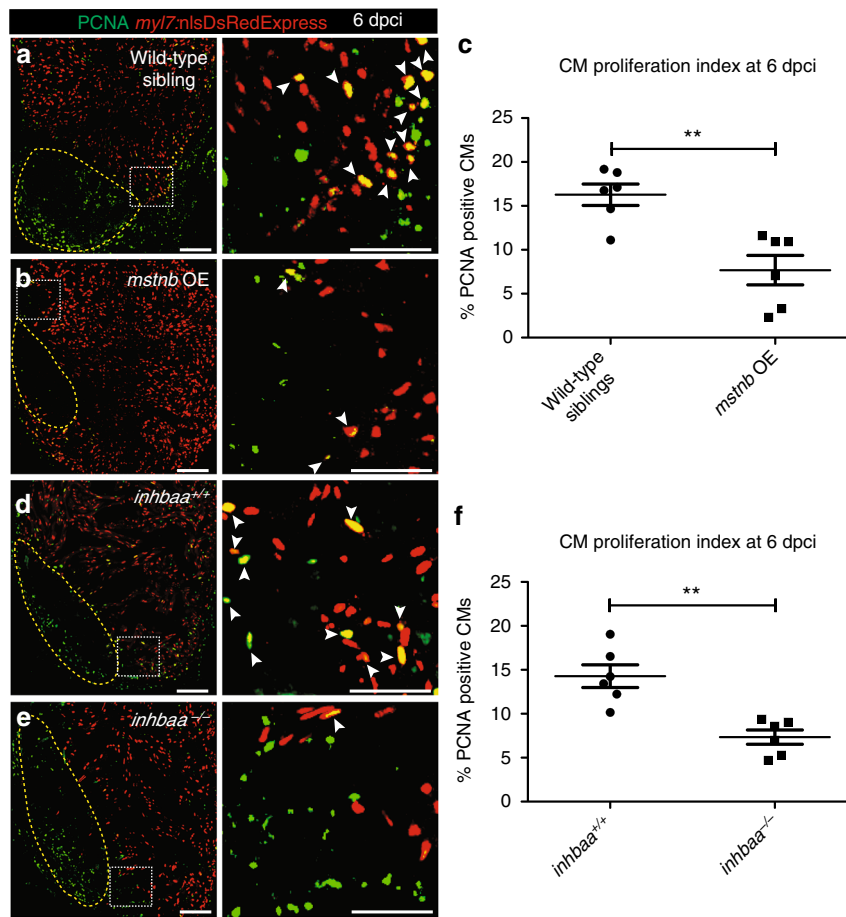


Fig. 2 *mstnb* GOF and *inhbaa* LOF suppress CM proliferation during cardiac regeneration. **a, b** Sections of wild-type sibling and *mstnb* OE cryoinjured hearts in *Tg(myl7:nlsDsRedExpress)* background at 6 dpci; α -DsRed (red), PCNA (green). Yellow dotted regions delineate the injured area. Higher magnifications of dashed boxes in **a, b** are shown on right side. White arrowheads point to proliferating CMs (PCNA⁺/DsRed⁺). **c** Quantification of CM proliferation in wild-type sibling ($n = 6$) and *mstnb* OE ($n = 6$) cryoinjured hearts in the 100 μ m region adjacent to the injured area at 6 dpci. **d, e** Sections of *inhbaa*^{+/+} and *inhbaa*^{-/-} cryoinjured hearts in *Tg(myl7:nlsDsRedExpress)* background at 6 dpci; α -DsRed (red), PCNA (green). Higher magnifications of dashed boxes in **d, e** are shown on right side. **f** Quantification of CM proliferation in *inhbaa*^{+/+} ($n = 6$) and *inhbaa*^{-/-} ($n = 6$) cryoinjured hearts in the 100 μ m region adjacent to the injured area at 6 dpci. All cell counts were performed on three sections from each heart. Each data point on dot plot represents one heart (data are mean \pm s.e.m., ** $P \leq 0.01$ —Student's *t* test, two-tailed). Scale bars: heart sections, 100 μ m; higher magnifications, 50 μ m

by RT-qPCR (Supplementary Fig. 1o), suggesting active mRNA degradation. Similar to *mstnb* OE animals, *inhbaa*^{-/-} zebrafish do not exhibit any gross morphological defects and their hearts appear indistinguishable from those of wild-type siblings (Supplementary Fig. 1p–s), indicating that *inhbaa* does not play a critical role during zebrafish development.

The zebrafish heart responds to cardiac injury with the formation of a transient fibrotic scar, which is progressively replaced by newly formed healthy myocardium within two months⁷. To assess any possible defect in the process of cardiac regeneration, we tested for scar resolution in cryoinjured *mstnb* OE and *inhbaa*^{-/-} hearts at 45 dpci. By performing acid fuchsin orange G (AFOG) staining on sections, we observed that 45 dpci *mstnb* OE and *inhbaa*^{-/-} hearts were unable to resolve their scar, in contrast to wild-type siblings (Fig. 1i–l) of the same regenerative stage. These data show that both *mstnb* GOF and *inhbaa* LOF interfere with cardiac regeneration and consequently cause reduced scar clearance.

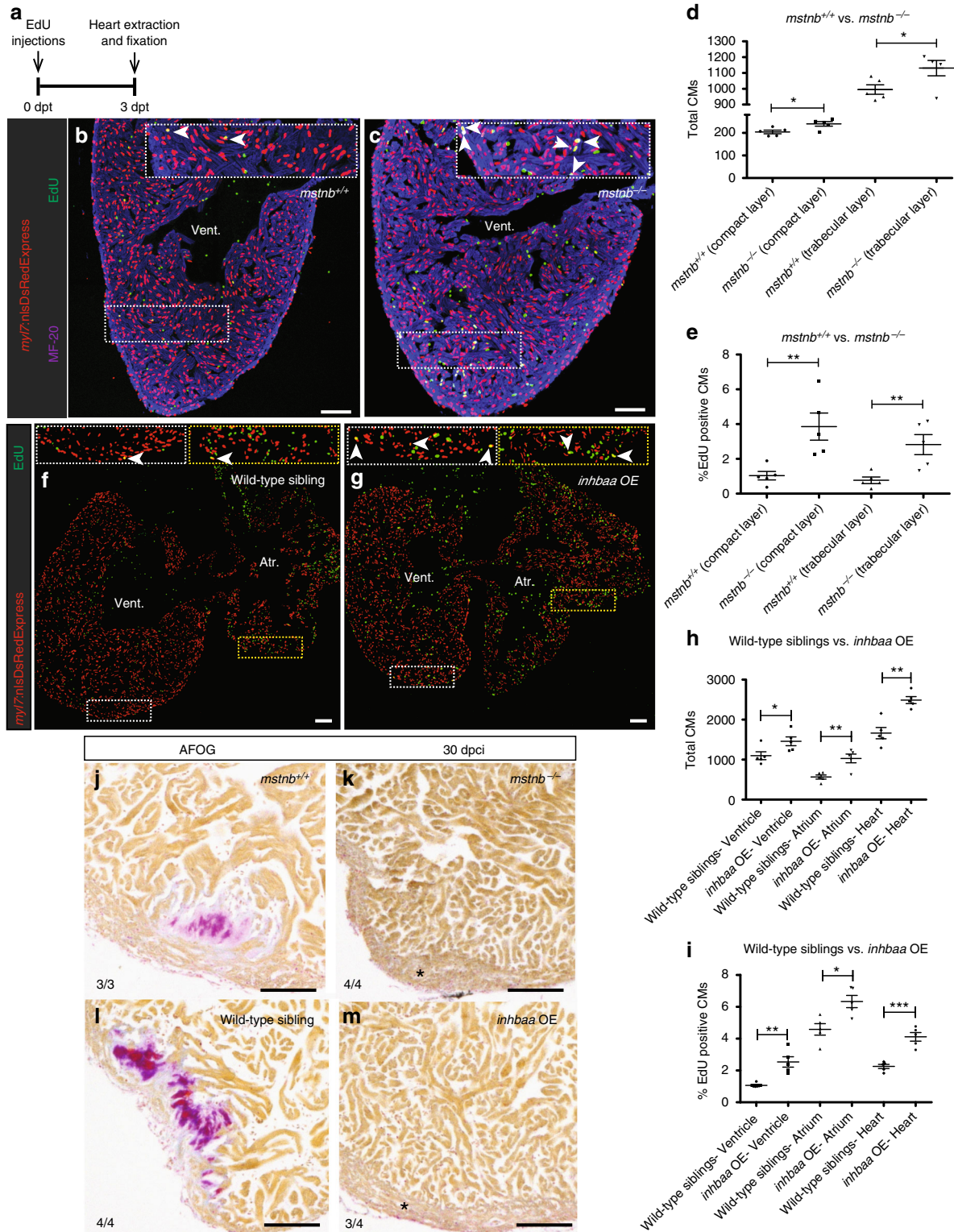
***mstnb* GOF and *inhbaa* LOF impair CM proliferation post injury.** Cardiac regeneration relies on the dedifferentiation and cell cycle re-entry of the spared CMs⁹. To test whether *inhbaa* deficiency or *mstnb* OE modulate CM dedifferentiation, we

assessed the expression of embryonic cardiac myosin heavy chain (embCMHC), a marker of dedifferentiated CMs⁴⁰, at 6 dpci. We could not observe any obvious differences in embCMHC expression in *mstnb* OE or *inhbaa*^{-/-} hearts compared to their wild-type siblings (Supplementary Fig. 2a–d). Next, we tested whether CM proliferation and cell cycle re-entry was affected in *mstnb* OE and *inhbaa*^{-/-} fish at 6 dpci. We used *Tg(myl7:nlsDsRedExpress)* fish and performed immunostaining for DsRed and PCNA (cell cycle stage marker), and quantified CM proliferation near the injured area. We observed a 53% ($\pm 13\%$ s.e.m.) decrease in CM proliferation in *mstnb* OE compared to control (Fig. 2a–c), suggesting that *mstnb* has a significant inhibitory effect on CM proliferation during cardiac regeneration. Similarly, we observed a 49% ($\pm 11.5\%$ s.e.m.) reduction in CM proliferation in *inhbaa*^{-/-} compared to *inhbaa*^{+/+} animals (Fig. 2d–f), indicating that *inhbaa* is instrumental for CM proliferation in the regenerating heart. Taken together, these results show that *mstnb* GOF and *inhbaa* LOF negatively affect CM proliferation, indicating that these two TGF- β family ligands have opposite functions during cardiac regeneration.

***mstnb* LOF and *inhbaa* GOF promote CM proliferation.** Further, as a complementary approach, we examined the effects of

mstnb LOF and *inhbaa* GOF on cardiac development and regeneration. In order to analyze the effect of the loss of *mstnb*, we generated *mstnb* mutant fish using a TALEN targeting the region after the signal peptide domain (Supplementary Fig. 3a) and recovered a 10 bp deletion allele, *mstnb^{bms5}* (Supplementary Fig. 3b), which is predicted to encode a truncated protein (Supplementary Fig. 3c). According to our RT-qPCR data, *mstnb* transcript levels are significantly reduced in *mstnb^{-/-}* compared to *mstnb^{+/+}* (Supplementary Fig. 3d), suggesting mRNA decay.

As previously reported in other species^{32, 33}, adult *mstnb^{-/-}* fish appear hypermuscular, suggesting a conserved function of *Mstn* in skeletal muscle growth. Interestingly, we also observed increased heart size in *mstnb^{-/-}* with a thickened ventricular wall (Supplementary Fig. 3e–j, l), the principal expression domain of *mstnb* as detailed previously. Notably, the eye size remained unaffected in *mstnb^{-/-}* compared to wild-type siblings (Supplementary Fig. 3k). To better understand whether the increase in ventricular wall thickness was a consequence of increased CM



proliferation in the compact layer, we injected EdU in adult *Tg(myl7:nlsDsRedExpress)* fish and performed immunostainings for DsRed and CM-specific myosin heavy chain (MF-20), followed by EdU labeling on cardiac sections (Fig. 3a). We quantified the total number of CMs as well as EdU incorporation in CMs in the compact and trabecular layers of the ventricle. Notably, hearts from *mstnb*^{-/-} animals showed a significant increase compared to siblings in the total number of CMs and the number of EdU incorporating CMs, in both the wall and the trabeculae of the ventricle (Fig. 3b–e). Our results therefore suggest that *mstnb* LOF promotes CM proliferation, leading to cardiac hyperplasia in zebrafish, unlike in *Mstn*-knockout mice which respond by cardiac hypertrophy^{34, 35}.

Next, we generated a transgenic zebrafish line for CM-specific constitutive OE of *inhbaa*, *Tg(myl7:inhbaa-2A-H2B-EGFP)* (*inhbaa* OE hereafter) (Supplementary Fig. 4a–c), resulting in strongly increased *inhbaa* transcript levels compared to control (Supplementary Fig. 4d). The majority of adult (3–6 months post fertilization (mpf)) *inhbaa* OE fish appear morphologically normal when compared to non-transgenic fish; however, the *inhbaa* OE hearts are significantly enlarged and show dense trabeculation in both chambers, whereas the eye size is unaffected (Supplementary Fig. 4e–k). During late adult stages (>6 mpf), we observed ~20% of the *inhbaa* OE fish developing pericardial edema with abnormally enlarged atria, indicating symptoms of a failing heart due to prolonged *inhbaa* OE. Further, to investigate the causality of cardiac enlargement and hypertrabeculation observed in *inhbaa* OE hearts of young adults, we performed EdU injections in adult *Tg(myl7:nlsDsRedExpress)* fish and immunostained for DsRed, followed by EdU labeling (Fig. 3a). Quantification of total number of CMs as well as EdU incorporation in CMs was performed for both chambers. We detected a significant increase in the total number of CMs, as well as in the number of EdU incorporating CMs in *inhbaa* OE hearts compared to control (Fig. 3f–i). Further, we tested whether increased CM proliferation helps these hearts after injury. Thus, we compared *mstnb*^{-/-} and *inhbaa* OE hearts with their siblings at 30 dpci, a time point at which wild-type cryoinjured hearts still retain scarring⁷. By performing AFOG staining on sections, we observed that 30 dpci *mstnb*^{-/-} and *inhbaa* OE hearts had completely resolved scars, in contrast to their wild-type siblings (Fig. 3j–m). Taken together, these results consolidate the finding that *mstnb* and *inhbaa* have opposing effects on CM proliferation during regeneration. Intriguingly, *inhbaa* OE and *mstnb* loss-of-function lead to CM hyperplasia, suggesting that *inhbaa* acts as a mitogen during development and repair.

inhbaa OE promotes CM proliferation independent of ErbB2.

To further investigate the pro-mitogenic effect of *inhbaa* OE on CMs, we analyzed CM proliferation in larval hearts at 120 h post fertilization (hpf). CM labeling was achieved using the *Tg(myl7:nlsDsRedExpress)* background, which again was combined with an EdU incorporation assay, followed by immunostaining for

DsRed (Fig. 4a). We observed an increase of 35% ($\pm 11\%$ s.e.m.) in the number of EdU incorporating CMs in *inhbaa* OE larvae compared to control (Fig. 4b–d), indicating that *inhbaa* OE also promotes CM proliferation at early stages. We next wanted to analyze whether the effects of *inhbaa* OE on CM proliferation depended on the Nrg–ErbB signaling pathway, a well-known regulator of CM proliferation^{14–16}. Thus, we injected *myl7:inhbaa-2A-H2B-EGFP* and *myl7:H2B-EGFP* plasmid DNA in embryos from *erbb2*^{st61} heterozygote intercrosses and performed EdU incorporation analysis (Fig. 4e), followed by genotyping. Examining GFP⁺ CMs in *erbb2*^{st61} homozygous mutants at 120 hpf, we found that a significant amount of *erbb*^{-/-} CMs expressing *inhbaa* OE were EdU⁺ while *erbb*^{-/-} CMs expressing GFP alone did not show any signs of EdU incorporation (Fig. 4f–h). Next, we treated *inhbaa* OE larvae and wild-type siblings with the established ErbB2 inhibitor PD168393 and analyzed CM proliferation (Supplementary Fig. 5a). We observed that pharmacological inhibition of ErbB2 significantly reduced CM proliferation, as described previously¹⁶, and interestingly, that *inhbaa* OE was able to rescue this effect. We found that *inhbaa* OE induces an increase of 77.5% ($\pm 18\%$ s.e.m.) in the number of EdU incorporating CMs compared to wild-type siblings under ErbB2-blocking conditions (Supplementary Fig. 5b–d).

As recently reported, in zebrafish, Nrg2a signals through ErbB2 to induce CM trabeculation and proliferation¹⁷. We were interested to compare the effects of *inhbaa* and *nrg2a* OE, and thus decided to test whether the OE of both ligands resulted in an additive effect on CM proliferation. Thus, by crossing *inhbaa* OE and *Tg(myl7:nrg2a-p2a-tdTomato)* (*nrg2a* OE hereafter) fish, we analyzed CM proliferation in 120 hpf *Tg(myl7:nlsDsRedExpress)* larvae, by performing immunostaining for DsRed, followed by EdU labeling (Fig. 4i) and genotyping. As expected from our before-mentioned observations and recently published work¹⁷, there was an increase of 38% ($\pm 7.5\%$ s.e.m.) and 55% ($\pm 8\%$ s.e.m.) in the number of EdU incorporating CMs in *inhbaa* OE and *nrg2a* OE larvae, respectively (Fig. 4j–l, n). However, we did not observe any additive effects from overexpressing both ligands, which resulted in a 53% ($\pm 6\%$ s.e.m.) increase in the number of EdU incorporating CMs, similar to *nrg2a* OE alone (Fig. 4m, n). This result might indicate that CM proliferation reaches its maximum by *nrg2a* OE alone, as supported by the minimal variability across the assessed samples, or an interference of *Inhbaa*-mediated proliferation by ErbB signaling. Altogether, these data show that *Inhbaa* can promote CM proliferation during development and without the need of regenerative stimuli, and that the mitogenic activity of *Inhbaa* on CMs acts independently of ErbB2 receptor activity.

***inhbaa* and *mstnb* compete to regulate CM proliferation.** Next, to investigate whether *mstnb* and *inhbaa* collaboratively regulate CM proliferation, we crossed our *inhbaa* OE line with the *mstnb* OE line in presence of the CM marking *Tg(myl7:nlsDsRedExpress)*

Fig. 3 *mstnb* LOF and *inhbaa* GOF positively affect physiological CM proliferation and cardiac regeneration. **a** Experimental setup of EdU treatment, followed by heart extraction and fixation. **b, c** Sections of *mstnb*^{+/+} and *mstnb*^{-/-} adult hearts in *Tg(myl7:nlsDsRedExpress)* background; α -DsRed (red), MF-20 (blue), EdU (green). Higher magnifications of dashed boxes in **b, c** are shown in upper right corners. White arrowheads point to EdU⁺/DsRed⁺ CMs. **d, e** Quantification of total CMs (DsRed⁺) and EdU incorporating CMs (EdU⁺/DsRed⁺) in the compact and trabecular layers of *mstnb*^{+/+} ($n = 5$) and *mstnb*^{-/-} ($n = 5$) ventricles. **f, g** Sections of wild-type sibling and *inhbaa* OE adult hearts in *Tg(myl7:nlsDsRedExpress)* background; α -DsRed (red), EdU (green). Higher magnifications of dashed boxes in **f, g** are shown in upper left and upper right corners. **h, i** Quantification of total CMs (DsRed⁺) and EdU incorporating CMs (EdU⁺/DsRed⁺) in wild-type sibling ($n = 5$) and *inhbaa* OE ($n = 5$) hearts. All cell counts were performed on three sections from each heart. Each data point on dot plot represents one heart (data are mean \pm s.e.m., * $P \leq 0.05$, ** $P \leq 0.01$, *** $P \leq 0.001$ —Student's *t* test, two-tailed). **j–m** AFOG staining of sections from *mstnb*^{+/+} ($n = 3$), *mstnb*^{-/-} ($n = 4$), wild-type sibling ($n = 4$), and *inhbaa* OE ($n = 4$) cryoinjured hearts at 30 dpci. Asterisks indicate the regions of resolved scarring. The numerators indicate the number of hearts with a particular pattern of scarring, and the denominators the total number of hearts analyzed. Scale bars, 100 μ m. dpt, days post treatment; vent., ventricle; atr., atrium

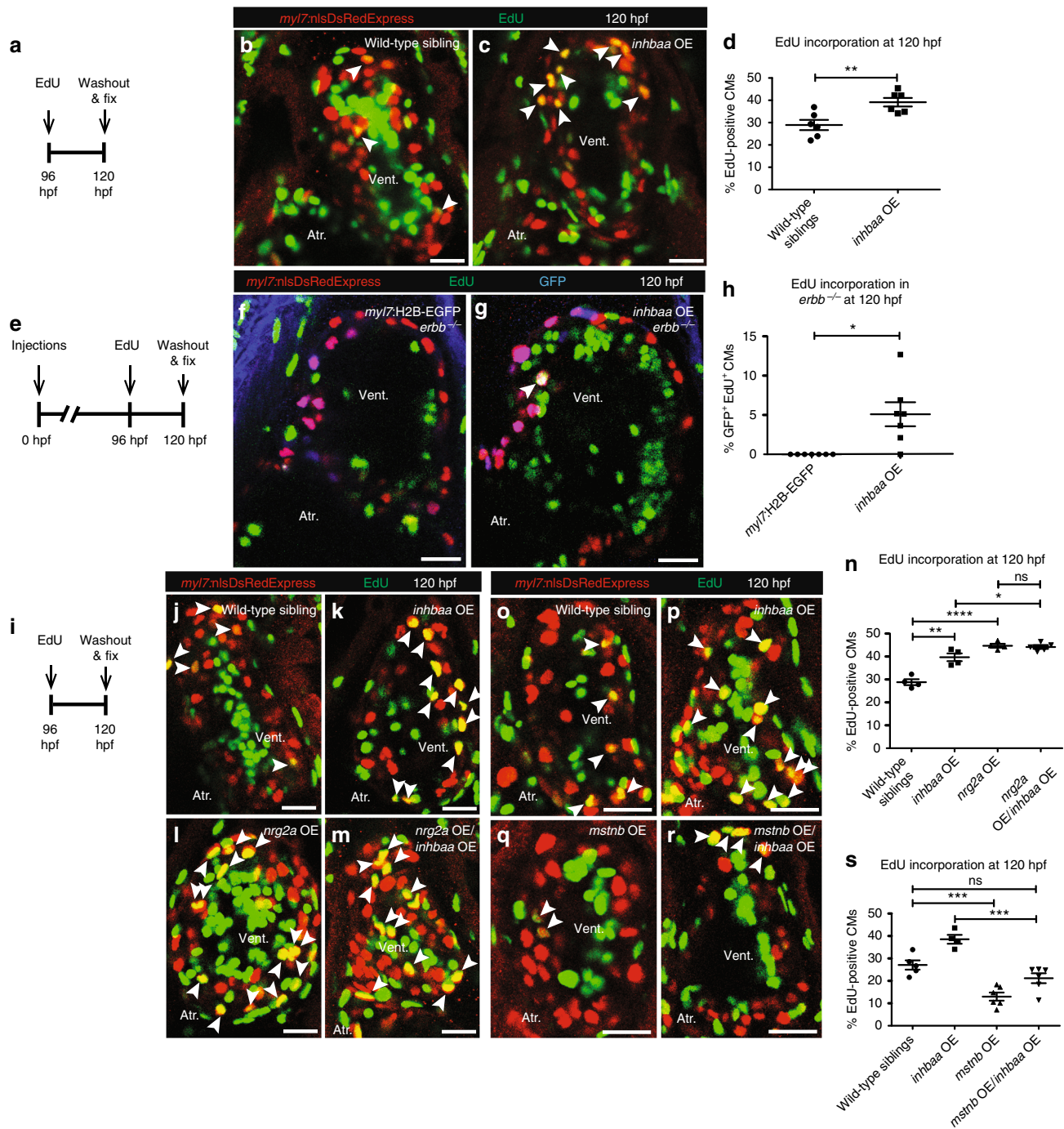
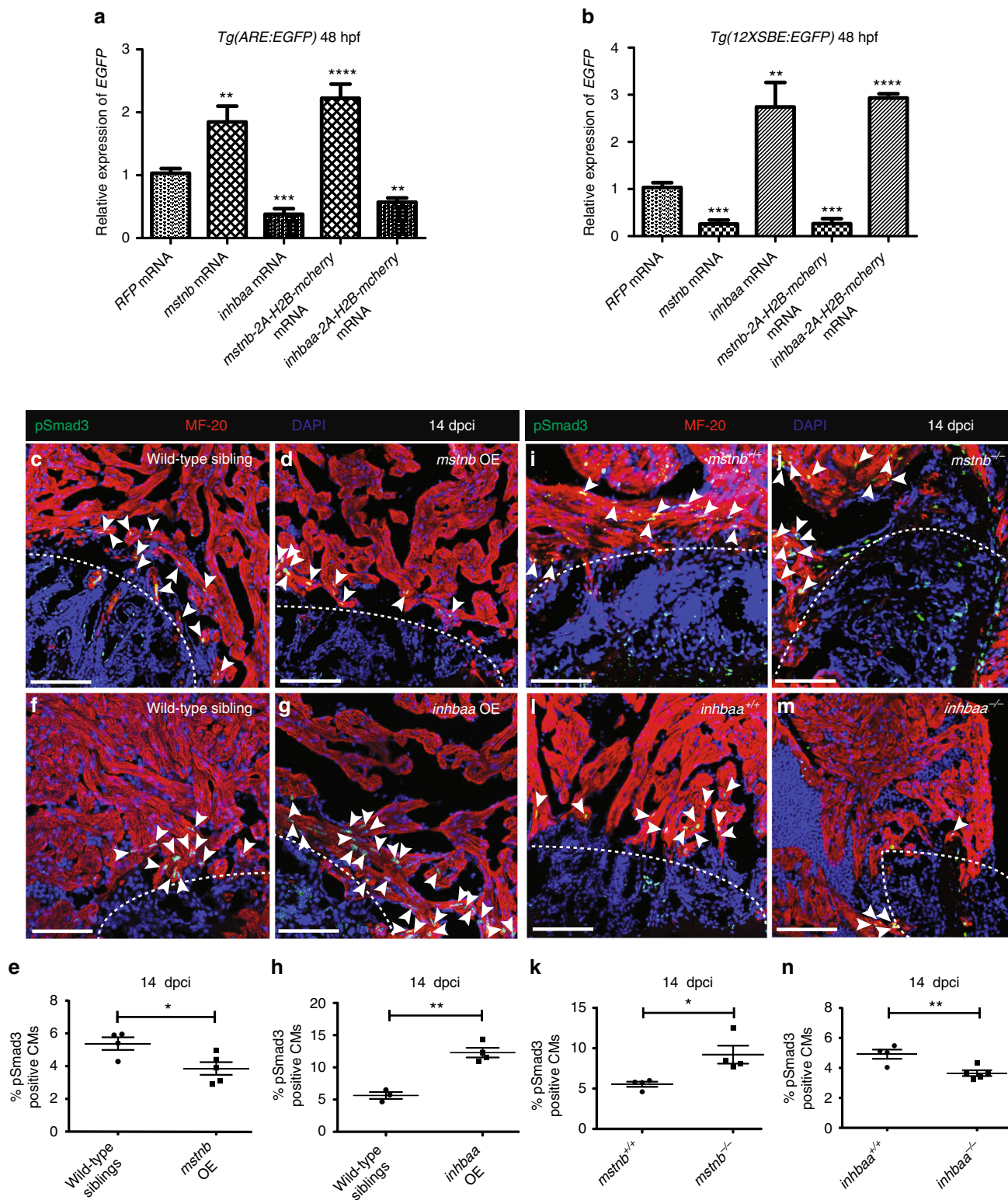


Fig. 4 *inhbaa* GOF promotes CM proliferation independently of ErbB2 signaling and competes with *mstnb* GOF. **a** Experimental setup of EdU treatment, followed by fixation. **b, c** *Tg(myl7:nlsDsRedExpress)* hearts of wild-type sibling and *inhbaa* OE larvae at 120 hpf; α -DsRed (red), EdU (green). White arrowheads point to proliferating CMs ($\text{EdU}^+/\text{DsRed}^+$). **d** Quantification of CM proliferation in wild-type sibling ($n = 6$) and *inhbaa* OE ($n = 6$) ventricles at 120 hpf. **e** Experimental setup of injections, EdU exposure, followed by fixation. **f, g** *Tg(myl7:nlsDsRedExpress)* hearts of *myl7:H2B-EGFP* and *myl7:inhbaa-2A-H2B-EGFP* (*inhbaa* OE) injected *erbb^{-/-}* larvae at 120 hpf; α -DsRed (red), α -GFP (blue), EdU (green). White arrowheads point to proliferating CMs ($\text{EdU}^+/\text{DsRed}^+/\text{GFP}^+$). **h** Quantification of CM proliferation in *myl7:H2B-EGFP* ($n = 7$) and *inhbaa* OE ($n = 7$) injected ventricles at 120 hpf. **i** Experimental setup of EdU treatment, followed by fixation. **j-m** *Tg(myl7:nlsDsRedExpress)* hearts of wild-type sibling, *inhbaa* OE, *nrg2a* OE, and *nrg2a* OE/*inhbaa* OE larvae at 120 hpf; α -DsRed (red), EdU (green). White arrowheads point to proliferating CMs ($\text{EdU}^+/\text{DsRed}^+$). **n** Quantification of CM proliferation in wild-type sibling ($n = 4$), *inhbaa* OE ($n = 4$), *nrg2a* OE ($n = 4$), and *nrg2a* OE/*inhbaa* OE ($n = 5$) ventricles at 120 hpf. **o-r** *Tg(myl7:nlsDsRedExpress)* hearts of wild-type sibling, *inhbaa* OE, *mstnb* OE, and *mstnb* OE/*inhbaa* OE larvae at 120 hpf; α -DsRed (red), EdU (green). White arrowheads point to proliferating CMs ($\text{EdU}^+/\text{DsRed}^+$). **s** Quantification of CM proliferation in wild-type sibling ($n = 5$), *inhbaa* OE ($n = 4$), *mstnb* OE ($n = 6$), and *mstnb* OE/*inhbaa* OE ($n = 6$) ventricles at 120 hpf. All cell counts were performed on non-overlapping confocal planes (thickness, 1 μm) (data are mean \pm s.e.m., ns: no significant changes observed, * $P < 0.05$, ** $P < 0.01$, *** $P < 0.001$ and **** $P < 0.0001$ —Student's *t* test, two-tailed). Scale bars, 20 μm . vent., ventricle; atr., atrium

background. Measuring EdU incorporation (Fig. 4i) followed by genotyping, we found that *mstnb* OE reduces myocardial EdU incorporation induced by *inhbaa* OE back to wild-type levels (Fig. 4o–s). Hence, our results suggest that *Mstnb* and *Inhbaa* compete in controlling CM cell cycle progression.

***mstnb* and *inhbaa* overexpression activate distinct Smads.** We further aimed to decipher the molecular mechanisms underlying

the differential regulation of CM proliferation and therefore, cardiac regeneration by *mstnb* and *inhbaa*. Myostatin and Activin have been reported to act through the TGF- β signaling cascade, leading to the phosphorylation of Smad2 and Smad3^{21, 22, 41}. Smad2, along with Smad4 and transcription factors such as FAST1/2, binds to the activin response elements (ARE) present in the promoter regions of target genes^{42–44}. Similarly, Smad3 binds to the Smad-binding elements (SBE) present in the promoter



region of target genes^{45, 46}. To identify potentially distinct transcriptional target genes of *Mstnb* and *Inhbaa* signaling, we used the published *Smad2* reporter line, *Tg(ARE:EGFP)*⁴⁷ and *Smad3* reporter line, *Tg(12XSBE:EGFP)*⁴⁸. After injecting *mstnb-2A-H2B-mcherry* and *inhbaa-2A-H2B-mcherry* mRNA in *Tg(ARE:EGFP)* and *Tg(12XSBE:EGFP)* embryos at the one-cell stage, we quantified *EGFP* mRNA expression at 48 hpf by RT-qPCR. Our results show a robust induction of *Smad2* reporter expression and a downregulation of *Smad3* reporter expression after *mstnb-2A-H2B-mcherry* mRNA injections (Fig. 5a, b). Conversely, we found that *inhbaa-2A-H2B-mcherry* mRNA injections induced *Smad3* reporter activity and suppressed *EGFP* mRNA expression in the *Smad2* reporter system (Fig. 5a, b). To make sure that our P2A-labeling strategy did not interfere with protein function and overall specificity, the aforementioned experiments were also performed with non-tagged wild-type versions leading to results identical in magnitude and specificity (Fig. 5a, b). This differential regulation of the activities of distinct *Smad* responsive elements by *mstnb* and *inhbaa* might account for their different influence on CM proliferation.

To further validate these results, we investigated the transcriptional response of several known TGF- β targets in response to *inhbaa* or *mstnb* OE. Several TGF- β target genes have been reported to be specific targets of *Smad2*, including *Gooseoid* (*Gsc*)⁴⁴ and *Mix.2*⁴³ or *Smad3*, including *JunB*⁴⁵ and *Plasminogen activator inhibitor-1(PAI-1)*⁴⁶. We thus analyzed the expression of these target genes (along with their paralogs) in 48 hpf *mstnb-2A-H2B-mcherry* mRNA and *inhbaa-2A-H2B-mcherry* mRNA injected embryos, by RT-qPCR. Interestingly, we found an upregulation of *Smad2* target gene expression by *mstnb* OE but a downregulation of their expression after *inhbaa* OE (Supplementary Fig. 6a–d). Conversely, we observed an upregulation of *Smad3* target gene expression by *inhbaa* OE but a downregulation of their expression after *mstnb* OE (Supplementary Fig. 6e–l). We further tested whether *mstnb* and *inhbaa* OE was able to regulate the expression of these *Smad* target genes in the injured adult heart. By performing RT-qPCR at 4 dpci, we found that the expression of *Smad2* target genes was induced in *mstnb* OE hearts, whereas either no significant effect or a transcriptional downregulation was observed in *inhbaa* OE hearts (Supplementary Fig. 7a–d). Conversely, *inhbaa* OE was able to induce the expression of *Smad3* target genes in regenerating hearts, whereas their expression was either unchanged or downregulated after *mstnb* OE (Supplementary Fig. 7e–l). These results further suggest that *Smad2* and *Smad3* activities are inversely regulated by *mstnb* and *inhbaa*.

***mstnb* and *inhbaa* inversely regulate *Smad3* phosphorylation.** *Smad3*-dependent TGF- β signaling has previously been linked to

cardiac regeneration as Activin type 1 receptor inhibition caused a reduction in the number of p*Smad3*⁺ CMs and ultimately blocked cardiac regeneration³¹. Additionally, by using the same chemical inhibitor, it has been shown that the inhibition of TGF- β signaling negatively affects CM proliferation in zebrafish⁴⁹. Thus, in order to test whether *mstnb* and *inhbaa* affect the phosphorylation of myocardial *Smad3* during cardiac regeneration, we performed immunostainings for p*Smad3* and MF-20 using a DAPI counterstain at 14 dpci, followed by quantification of p*Smad3*⁺ CMs proximal to injury site in the respective gain-of-function and loss-of-function genotypes. Interestingly, we found that OE of *mstnb* inhibits *Smad3* phosphorylation and detected a 28% ($\pm 10\%$ s.e.m.) decrease in the number of p*Smad3*⁺ CMs in *mstnb* OE compared to control (Fig. 5c–e). Conversely, OE of *inhbaa* induced myocardial *Smad3* phosphorylation, with an increase of 118% ($\pm 20\%$ s.e.m.) in the number of p*Smad3*⁺ CMs compared to control (Fig. 5f–h). Notably, we also observed that *mstnb*^{-/-} hearts show an induction of *Smad3* phosphorylation in CMs, with an increase of 66% ($\pm 21\%$ s.e.m.) in the number of p*Smad3*⁺ CMs compared to control (Fig. 5i–k). Further, we detected a decline of 26% ($\pm 7.5\%$ s.e.m.) in the number of p*Smad3*⁺ CMs in *inhbaa*^{-/-} compared to control (Fig. 5l–n), indicating that *Inhbaa* is important to induce *Smad3* phosphorylation during cardiac regeneration. Overall, our data indicate that *Mstnb* and *Inhbaa* act antagonistically to one another in controlling *Smad3* phosphorylation, an apparently crucial event during cardiac regeneration in zebrafish.

***Smad2* and *Smad3* inversely affect CM proliferation.** Myocardial *Smad3* phosphorylation is induced at the site of injury during cardiac regeneration³¹. Our data from regenerating *mstnb* OE and *inhbaa*^{-/-} hearts show that myocardial *Smad3* phosphorylation proximal to the lesion was reduced (Fig. 5c–e, l–n), as was CM proliferation. In order to test the hypothesis that *Smad3* phosphorylation is directly linked to CM proliferation, we used a small molecule inhibitor, SIS3, to block TGF- β -mediated *Smad3* phosphorylation^{50, 51}. By performing RT-qPCR, we first tested whether SIS3 acts as a specific inhibitor of *Smad3* phosphorylation, and found that *Smad3* target gene expression was downregulated in 72 hpf SIS3-treated hearts (Supplementary Fig. 8h–l), while *Smad2* target gene expression remained unchanged (Supplementary Fig. 8e–g). We also analyzed the effect of the established Activin type 1 receptor inhibitor (SB431542) on *Smad* target gene expression, by performing RT-qPCR in 72 hpf SB431542-treated hearts. We observed a downregulation in the expression of both *Smad2* and *Smad3* target genes (Supplementary Fig. 8e–l), confirming that this inhibitor blocks the complete TGF- β pathway as reported previously⁵². Next, we treated *Tg(myl7:nlsDsRedExpress)* larvae with SIS3 and analyzed CM

Fig. 5 *mstnb* and *inhbaa* inversely regulate the activities of *Smad2* and *Smad3* response elements, as well as *Smad3* phosphorylation. **a** RT-qPCR analysis for relative *EGFP* mRNA expression in 48 hpf *Tg(ARE:EGFP)* embryos injected with *mstnb*, *inhbaa*, *mstnb-2A-H2B-mcherry*, and *inhbaa-2A-H2B-mcherry* mRNA compared to *RFP* mRNA injected ($n = 2 \times 10$ embryos assessed as 2 biological and 2 technical replicates). **b** RT-qPCR analysis for relative *EGFP* mRNA expression in 48 hpf *Tg(12XSBE:EGFP)* embryos injected with *mstnb*, *inhbaa*, *mstnb-2A-H2B-mcherry*, and *inhbaa-2A-H2B-mcherry* mRNA compared to *RFP* mRNA injected ($n = 2 \times 10$ embryos assessed as two biological and two technical replicates). **c, d** Sections of wild-type sibling and *mstnb* OE cryoinjured hearts at 14 dpci; p*Smad3* (green), α -MF-20 (red), DAPI (blue). White dotted regions delineate the injured area. White arrowheads point to p*Smad3*⁺ CMs near the injured area. **e** Quantification of p*Smad3*⁺ CMs in wild-type sibling ($n = 4$) and *mstnb* OE ($n = 5$) cryoinjured hearts in the 100 μ m region adjacent to the injured area at 14 dpci. **f, g** Sections of wild-type sibling and *inhbaa* OE cryoinjured hearts at 14 dpci; p*Smad3* (green), α -MF-20 (red), DAPI (blue). **h** Quantification of p*Smad3*⁺ CMs in wild-type sibling ($n = 3$) and *inhbaa* OE ($n = 4$) cryoinjured hearts in the 100 μ m region adjacent to the injured area at 14 dpci. **i, j** Sections of *mstnb*^{+/+} and *mstnb*^{-/-} cryoinjured hearts at 14 dpci; p*Smad3* (green), α -MF-20 (red), DAPI (blue). **k** Quantification of p*Smad3*⁺ CMs in *mstnb*^{+/+} ($n = 4$) and *mstnb*^{-/-} ($n = 4$) cryoinjured hearts in the 100 μ m region adjacent to the injured area at 14 dpci. **l, m** Sections of *inhbaa*^{+/+} and *inhbaa*^{-/-} cryoinjured hearts at 14 dpci; p*Smad3* (green), α -MF-20 (red), DAPI (blue). **n** Quantification of p*Smad3*⁺ CMs in *inhbaa*^{+/+} ($n = 4$) and *inhbaa*^{-/-} ($n = 5$) cryoinjured hearts in the 100 μ m region adjacent to the injured area at 14 dpci. All cell counts were performed on three sections from each heart. Each data point on dot plot represents one heart (data are mean \pm s.e.m., * $P \leq 0.05$, ** $P \leq 0.01$, *** $P \leq 0.001$ and **** $P \leq 0.0001$ —Student's *t* test, two-tailed). Scale bars, 100 μ m

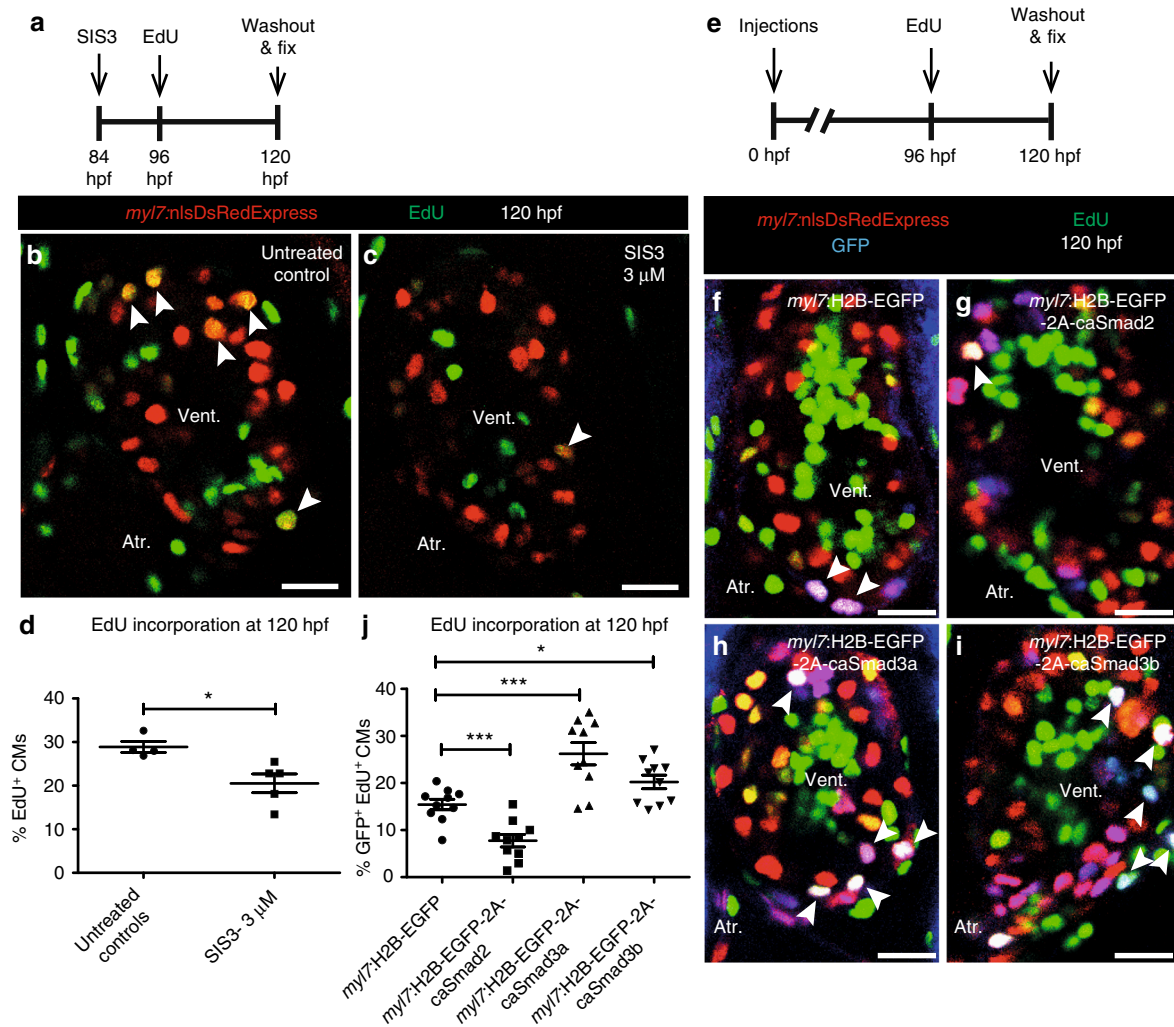


Fig. 6 CM proliferation is inversely regulated by Smad2 and Smad3. **a** Experimental setup of SIS3 treatment, followed by EdU treatment and fixation. **b, c** *Tg(myl7:nlsDsRedExpress)* hearts of untreated control and 3 μ M SIS3-treated larvae at 120 hpf; α -DsRed (red), EdU (green). White arrowheads point to proliferating CMs (EdU⁺/DsRed⁺). **d** Quantification of CM proliferation in untreated control ($n = 4$) and 3 μ M SIS3-treated hearts at 120 hpf. **e** Experimental setup of injections, followed by EdU treatment and fixation. **f–i** *Tg(myl7:nlsDsRedExpress)* hearts of *myl7:H2B-EGFP*, *myl7:H2B-EGFP-2A-caSmad2*, *myl7:H2B-EGFP-2A-caSmad3a* and *myl7:H2B-EGFP-2A-caSmad3b* injected larvae at 120 hpf; α -DsRed (red), α -GFP (blue), EdU (green). White arrowheads point to proliferating CMs (EdU⁺/DsRed⁺/GFP⁺). **j** Quantification of CM proliferation in *myl7:H2B-EGFP* ($n = 10$), *caSmad2* ($n = 10$), *caSmad3a* ($n = 10$), and *caSmad3b* ($n = 10$) injected ventricles at 120 hpf. All cell counts were performed on non-overlapping confocal planes (thickness, 1 μ m) (data are mean \pm s.e.m., * $P < 0.05$ and *** $P \leq 0.001$ —Student's *t* test, two-tailed). Scale bars, 20 μ m. vent., ventricle; atr., atrium

proliferation by performing immunostaining for DsRed, followed by EdU labeling at 120 hpf (Fig. 6a). Quantification of EdU incorporation in CMs of larval ventricles revealed that 3 μ M SIS3 was sufficient to substantially reduce the number of EdU⁺ CMs (Fig. 6b–d), suggesting that CM proliferation relies on Smad3 phosphorylation.

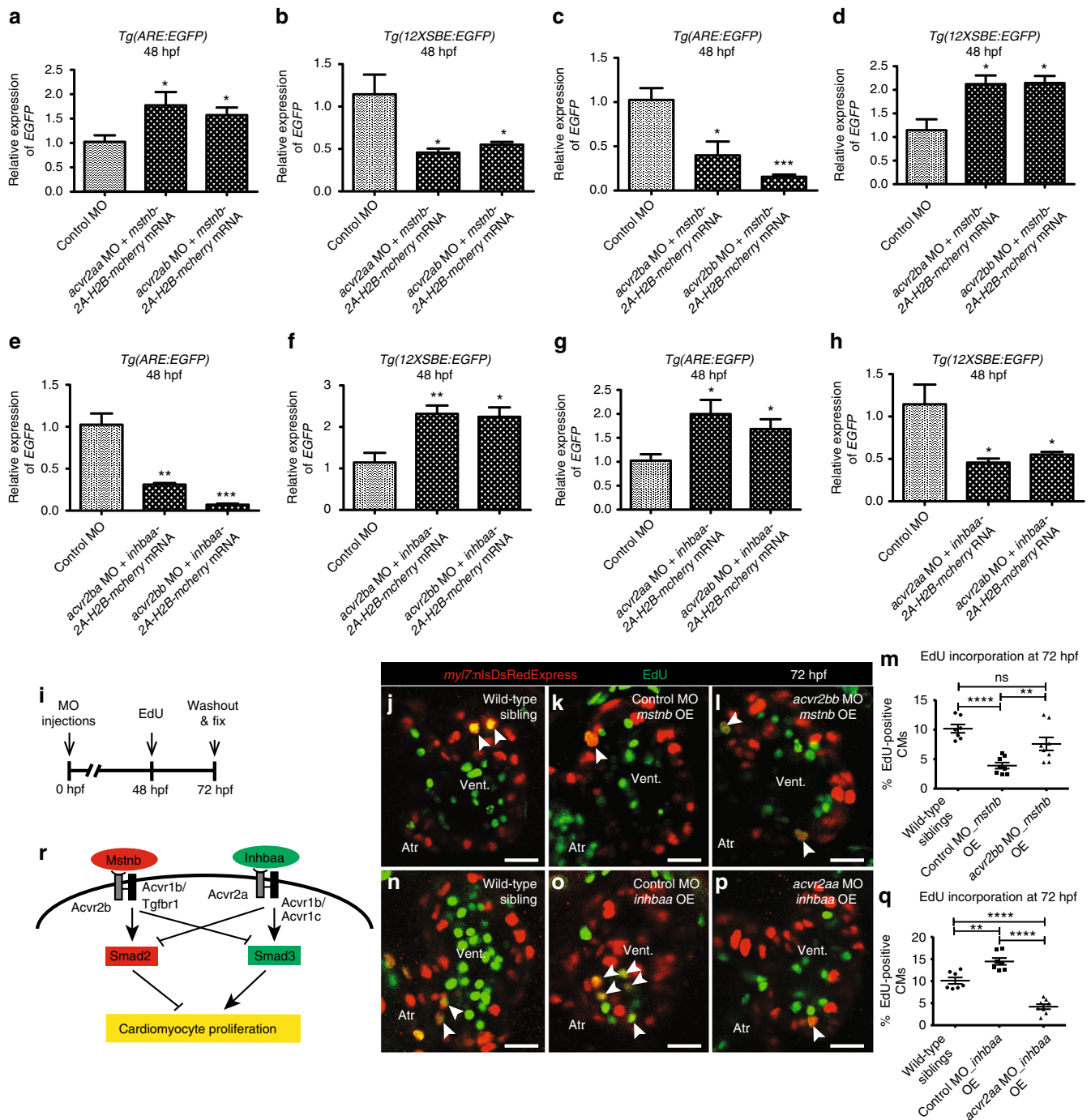
To further test our model, we analyzed the effects of constitutively active (ca) Smad2, Smad3a and Smad3b on CM proliferation following mosaic OE. For this analysis, we generated constructs expressing ca, phosphomimetic, Smads under the CM-specific *myl7* promoter, namely *Tg(myl7:H2B-EGFP-2A-caSmad2)* (*caSmad2* hereafter), *Tg(myl7:H2B-EGFP-2A-caSmad3a)* (*caSmad3a* hereafter), *Tg(myl7:H2B-EGFP-2A-caSmad3b)* (*caSmad3b* hereafter), and *Tg(myl7:H2B-EGFP)* as control (Supplementary Fig. 8a–d). We first tested whether the *caSmad2*, *caSmad3a*, and *caSmad3b* constructs were functional and specific, by performing RT-qPCR analysis for Smad2 and Smad3 target gene expression on hearts of 72 hpf larvae obtained from outcrossing the *caSmad2*, *caSmad3a*, and *caSmad3b* founders. We observed an upregulation

in Smad2 target gene expression in *caSmad2* hearts (Supplementary Fig. 8e–g), and an upregulation in Smad3 target gene expression in *caSmad3a* and *caSmad3b* hearts (Supplementary Fig. 8h–l). After injection of the constructs at the one-cell stage, we analyzed CM proliferation by performing immunostaining for GFP and DsRed, followed by EdU labeling in 120 hpf *Tg(myl7:nlsDsRedExpress)* larvae (Fig. 6e). Comparing GFP⁺ CMs across all constructs, we found that CMs expressing *caSmad2* showed a 50% ($\pm 12\%$ s.e.m.) reduction in EdU incorporation compared to CMs expressing GFP alone, whereas both *caSmad3a* and *caSmad3b* expression resulted in a 70% ($\pm 18\%$ s.e.m.) and 31% ($\pm 12\%$ s.e.m.) increase in EdU incorporation, respectively (Fig. 6f–j). These results clearly indicate that Smad2 and Smad3 inversely regulate CM proliferation in zebrafish and could potentially explain how different TGF- β family ligands can have opposite effects during regeneration.

Mstnb and Inhba signal through distinct Activin receptors. Mstn and Inhba have been described to signal through the same

type 2 receptor complex^{21, 22, 41}. We wanted to investigate how *Mstnb* and *Inhbaa* could function antagonistically if they work through the same signaling cascade. Thus, to better understand the ligand-receptor relationships, we performed combined gene knockdown and OE experiments. We co-injected morpholinos (MOs) for the activin type 2 receptor genes (*acvr2aa*, *acvr2ab*, *acvr2ba*, and *acvr2bb*) with *mstnb-2A-H2B-mcherry* mRNA or *inhbaa-2A-H2B-mcherry* mRNA in the *Smad2*⁴⁷ and *Smad3*⁴⁸ reporter lines. By performing RT-qPCR for *EGFP* mRNA expression, we found that co-injection of *acvr2a* MOs (*acvr2aa* and *acvr2ab*) along with *mstnb* mRNA injections, since *Smad2* reporter expression was induced and *Smad3* reporter expression was

suppressed compared to control (Fig. 7a, b). In contrast, the co-injection of *acvr2b* MOs (*acvr2ba* and *acvr2bb*) along with *mstnb-2A-H2B-mcherry* mRNA significantly reduced the effect of *mstnb* OE on *Smad2* and *Smad3* reporter activity (Fig. 7c, d). These results indicate that *Mstnb* has a preference for binding *Acvr2b* over *Acvr2a*, as per previous studies^{41, 53}. Next, we tested the relationship between *Inhbaa* and *Acvr2ba* and *Acvr2bb*. We found that the co-injection of *acvr2b* MOs (*acvr2ba* and *acvr2bb*) with *inhbaa-2A-H2B-mcherry* mRNA did not influence the effect of *inhbaa* OE, as *Smad2* reporter expression was suppressed and *Smad3* reporter expression was induced compared to control (Fig. 7e, f). In contrast, the co-injection of *acvr2a* MOs (*acvr2aa* and *acvr2ab*) along with *inhbaa-2A-H2B-mcherry* mRNA significantly reduced the effect of



inhbaa OE on Smad2 and Smad3 reporter activity (Fig. 7g, h). These data suggest a previously unreported preference for *Inhbaa* to signal through *Acvr2a* over *Acvr2b*.

Finally, we also analyzed the effect of these receptor knock-downs in the CM EdU incorporation assay using our *mstnb* OE and *inhbaa* OE lines (Fig. 7i). Since its effect on Smad2 reporter expression was more significant compared to *acvr2ba* MO, we injected the *acvr2bb* MO in the *mstnb* OE line and assessed CM EdU incorporation at 72 hpf. We observed a significant increase of 94% ($\pm 33\%$ s.e.m.) in CM EdU incorporation in *acvr2bb* MO-injected *mstnb* OE larvae compared to control (Fig. 7j–m). This result is in line with our RT-qPCR data that *Acvr2b* is a specific receptor for *Mstnb*, and knocking down *acvr2bb* prevents the suppression of CM proliferation by *mstnb* OE. Next, we injected *acvr2aa* MO in the *inhbaa* OE line and examined CM EdU incorporation at 72 hpf. Here, we observed a significant reduction of 70% ($\pm 8\%$ s.e.m.) in CM EdU incorporation in *acvr2aa* MO-injected *inhbaa* OE larvae compared to control (Fig. 7n–q). Again, this result is in line with our RT-qPCR data that *Acvr2a* is a specific receptor for *Inhbaa*, and knocking down *acvr2aa* prevents the induction of CM proliferation by *inhbaa* OE. Overall, our results suggest that *Mstnb* binds to *Acvr2b*, leading to the activation of *Acvr1b/Tgfr1*, which promotes Smad2 and suppresses Smad3 activation. Inversely, *Inhbaa* binds to *Acvr2a*, leading to the activation of *Acvr1b/Acvr1c*, which promotes Smad3 and suppresses Smad2 activation (Fig. 7r).

Discussion

The role of TGF- β signaling in organ regeneration and pathology remains unclear as seemingly contradictory results have been reported. TGF- β signaling is required for the formation of the wound epithelium and cell proliferation during *Xenopus* tail regeneration⁵⁴, while its loss has been associated with an expansion of progenitor cells in the regenerating mammalian liver⁵⁵. Furthermore, TGF- β signaling has been implicated in the pathogenesis of cardiac remodeling and fibrosis after pressure overload in mammals³⁰, while the treatment of adult zebrafish with a TGF- β receptor inhibitor blocked cardiac regeneration³¹. Thus, because of its highly diverse and seemingly contradictory functions across various cell types and organisms, we wanted to dissect the role of different TGF- β family members in cardiac regeneration by performing ligand-specific genetic manipulations.

Here, we have identified the opposing expression response of two TGF- β family ligand encoding genes, *mstnb* and *inhbaa*. From subsequent genetic studies we have revealed their contrasting roles in regulating cardiac regeneration and CM proliferation in zebrafish. Our study shows that expression of *mstnb*,

a negative regulator of skeletal muscle growth^{32, 33}, is rapidly and continuously downregulated during cardiac regeneration in the adult zebrafish heart. However, this observation contrasts previous findings in mammals which show a rapid and significant upregulation of MSTN post MI²⁵. We therefore hypothesized that *mstnb* downregulation in zebrafish following cardiac injury facilitates cardiac regeneration, whereas elevated MSTN levels in the injured mammalian heart could possibly inhibit the process of regeneration. Supporting our hypothesis, we observed that loss of *mstnb* positively affects physiological CM proliferation and cardiac regeneration. Contrarily, *mstnb* OE in CMs led to a significant decline in CM proliferation, reduced regeneration and compromised scar clearance after injury. Overall, our data strongly support that *mstnb* downregulation is important during cardiac regeneration, facilitating CM proliferation.

In contrast, we have found that *inhbaa* expression was upregulated in response to cardiac injury during the early stages of myocardial regeneration. Further, the loss of *inhbaa* strongly correlated with reduced scar clearance and CM proliferation within the proximity of the injury site. Intriguingly, CM-specific *inhbaa* OE not only enhanced cardiac regeneration, but also resulted in cardiomegaly as a consequence of increased CM proliferation and hypertrabeculation, even in the absence of cardiac injury. The cardiac hypertrabeculation phenotype of the *inhbaa* OE fish is reminiscent of that observed in mice mutant for FKBP12⁵⁶, a negative regulator of the TGF- β family⁵⁷, suggesting a conserved function of TGF- β signaling in cardiac development and possibly CM proliferation. Recent reports have identified *Nrg* as a potent mitogen in fish and mammals^{4, 14, 17}. We performed epistasis experiments to test whether *inhbaa*-induced CM proliferation depends upon *Nrg*–ErbB signaling. These experiments revealed that *Inhbaa* stimulates CM proliferation independently of ErbB receptor activity, indicating that similar to *Nrg*, *Inhbaa* has the potential to induce CM proliferation directly. However, simultaneous OE of *nrg2a* and *inhbaa* did not yield a higher CM proliferative index than OE of *nrg2a* alone. Possibly, stimulation of CM proliferation becomes saturated by *nrg2a* OE alone, as suggested by the minimal variability observed across the different specimens. Alternatively, *Nrg2a* signaling might interfere with the potential of *Inhbaa* to promote CM proliferation. Indeed, stimulation of the MAPK signaling cascade by oncogenic mutations in Ras or by EGF receptor stimulation mediates the phosphorylation of specific residues in the linker region of Smad2/3⁵⁸. Phosphorylation of this linker region was shown to inhibit TGF- β -induced C-terminal phosphorylation and nuclear accumulation of Smads, attenuating the transcriptional activation of their target genes⁵⁸. Interestingly, *inhbaa* is upregulated after cardiac injury, both in mammals²⁶ and zebrafish, but potentially the timing and

Fig. 7 *Mstnb* and *Inhbaa* work through distinct Activin type 2 receptors to regulate CM proliferation. **a–d** RT-qPCR analysis for relative *EGFP* mRNA expression in 48 hpf *Tg(ARE:EGFP)* and *Tg(12XSBE:EGFP)* embryos injected with *acvr2aa* MO/*mstnb*-2A-H2B-mcherry mRNA, *acvr2ab* MO/*mstnb*-2A-H2B-mcherry mRNA, *acvr2ba* MO/*mstnb*-2A-H2B-mcherry mRNA, and *acvr2bb* MO/*mstnb*-2A-H2B-mcherry mRNA compared to control MO injected ($n = 2 \times 10$ embryos assessed as two biological and two technical replicates). **e–h** RT-qPCR analysis for relative *EGFP* mRNA expression in 48 hpf *Tg(ARE:EGFP)* and *Tg(12XSBE:EGFP)* embryos injected with *acvr2ba* MO/*inhbaa*-2A-H2B-mcherry mRNA, *acvr2bb* MO/*inhbaa*-2A-H2B-mcherry mRNA, *acvr2aa* MO/*inhbaa*-2A-H2B-mcherry mRNA, and *acvr2ab* MO/*inhbaa*-2A-H2B-mcherry mRNA compared to control MO-injected ($n = 2 \times 10$ embryos assessed as two biological and two technical replicates). **i** Experimental setup of injections, followed by EdU treatment and fixation. **j–l** *Tg(my17:nlsDsRedExpress)* hearts of wild-type sibling, control MO-injected *mstnb* OE and *acvr2bb* MO-injected *mstnb* OE larvae at 72 hpf; α -DsRed (red), EdU (green). White arrowheads point to proliferating CMs (EdU⁺/DsRed⁺). **m** Quantification of CM proliferation in wild-type sibling ($n = 7$), control MO-injected *mstnb* OE ($n = 8$) and *acvr2bb* MO-injected *mstnb* OE ($n = 8$) ventricles at 72 hpf. **n–p** *Tg(my17:nlsDsRedExpress)* hearts of wild-type sibling, control MO-injected *inhbaa* OE, and *acvr2aa* MO-injected *inhbaa* OE larvae at 72 hpf; α -DsRed (red), EdU (green). **q** Quantification of CM proliferation in wild-type sibling ($n = 7$), control MO-injected *inhbaa* OE ($n = 7$) and *acvr2aa* MO-injected *inhbaa* OE ($n = 8$) ventricles at 72 hpf. **r** Model of ligand-receptor relationship: *Mstnb* binds to *Acvr2b*, leading to the activation of *Acvr1b/Tgfr1*, which promotes Smad2 and suppresses Smad3 activation. Inversely, *Inhbaa* binds to *Acvr2a*, recruiting *Acvr1b/Acvr1c*, thereby inducing Smad3 and suppressing Smad2 activation. This process is followed by the differential regulation of CM proliferation by Smad2 and Smad3. All cell counts were performed on non-overlapping confocal planes (thickness, 1 μ m) (data are mean \pm s.e.m., ns: no significant changes observed, * $P \leq 0.05$, ** $P \leq 0.01$, *** $P \leq 0.001$ and **** $P \leq 0.0001$ —Student's *t* test, two-tailed). Scale bars, 20 μ m. vent., ventricle; atr., atrium

levels of its induction do not allow it to induce regeneration in the mammalian heart. In mammals, prolonged upregulation of *INHBA* has been associated with induction of fibrosis post MI, leading to cardiac remodeling and failure²⁶. We speculate that a transient upregulation of *INHBA* in injured hearts, as observed in zebrafish, along with a rapid inactivation of *MSTN* could be beneficial to stimulate CM proliferation while prolonged *INHBA* expression has negative consequences. Indeed, several of our *inhbaa* OE animals showed signs of cardiomyopathy and heart failure past 6 months of age, an effect that could be potentiated by the presence of a higher number of myofibroblasts and other non-myocardial cells in the mammalian heart⁵⁹.

Canonically, TGF- β family ligands including Myostatin and Activin signal through Activin type 2 and type 1 receptors leading to the C-terminal phosphorylation of Smad2 and Smad3. Mechanistically, it has been reported that Myostatin has a binding preference for the Activin type 2 receptor Acvr2b compared to Acvr2a^{41, 53}. We experimentally validated that not only Mstnb, but also *Inhbaa*, have different binding affinities for Activin type 2 receptors and inversely modulate the activities of Smad2 and Smad3. Smad2 and Smad3 have highly homologous MH1 and MH2 domains; however, the MH1 domain of Smad2 has 30 extra amino acids preventing its direct binding to DNA, unlike Smad3 which can directly bind to target DNA sequences⁶⁰. These structural differences in Smad2 and Smad3 may account for differences in their functions. Several recent studies have revealed the antagonistic effects of Smad2 and Smad3 during multiple cellular processes such as blastema formation in regeneration, tumor angiogenesis, and neurogenesis^{51, 61, 62}. Similarly, our data suggest that constitutively active Smad2 and Smad3 act antagonistically to one another in regulating CM proliferation. Additionally, we identified differential effects of *mstnb* and *inhbaa* OE on myocardial Smad3 phosphorylation in the regenerating heart, suggesting that indeed these two ligands are inversely affecting Smad3 phosphorylation which seemingly mediates CM proliferation during cardiac regeneration. Taken together, we identified opposite functions for the two TGF- β family ligands, Mstnb and *Inhbaa*, during cardiac regeneration and similarly, for their downstream effectors Smad2 and Smad3. In addition, the Nrg-ErbB independent mitogenic activity of *Inhbaa* may provide new avenues towards developing alternative strategies in the treatment of patients post MI.

Methods

Zebrafish. Procedures involving animals were approved by the veterinary department of the Regional Board of Darmstadt.

Zebrafish husbandry. All zebrafish husbandry was performed under standard conditions in accordance with institutional (MPG) and national ethical and animal welfare guidelines. The characterized mutant and transgenic lines *erbb2^{st6163}*, *Tg(-0.8myl7:nlDsRedExpress)hsc4⁶⁴*, *Tg(myl7:nrg2a202-p2a-tdTomato)bnsl140¹⁷*, *Tg(ARE:EGFP)fc100⁴⁷*, and *Tg(12XSBE:EGFP)ia16⁴⁸* were used in this study.

Cryoinjury. To perform cryoinjury⁷, adult zebrafish (3–6 mpf) were anaesthetized in 0.016% tricaine and placed on a wet sponge with their ventral side up. An incision was made through the chest to access the heart and a precooled cryoprobe was applied to the ventricular apex till the cryoprobe thawed. Later, the fish were recovered by transferring them to the fresh water.

Microarray expression profiling. Total RNA was isolated from ~6 mpf sham operated and cryoinjured hearts 4 dpci using Trizol (Life Technologies). Dual color cDNA labeling and hybridization was performed by *MOgene* (commercial service) using the Agilent Zebrafish (V3) 4 × 44 K platform. Microarray raw and normalized data have been submitted to NCBI-GEO under the accession number GSE89259.

LMD. LMD (LMD-6000, Leica) was performed on adult zebrafish heart cryosections to dissect the wall and trabecular tissues separately for RNA extraction.

Larval heart extraction. To perform heart extraction⁶⁵, 72 hpf larvae expressing GFP under CM-specific myosin, light chain 7, regulatory (*myl7*) promoter were anesthetized and transferred to 1.5 ml microfuge tube, followed by washing three times with embryo disruption medium (EDM) and resuspension in EDM. Further, 1 ml of EDM containing larvae was drawn into the 19-gauge needle and ejected back into the microfuge tube 30 times at the rate of 1 s per syringe medium. Fragmented larvae were passed through 100 μ m nylon mesh and the flow-through was collected in the petri dish. Later, the flow-through was passed through 40 μ m nylon mesh. Next, the mesh was inverted and the retained material was washed off with EDM into the petri dish. Intact GFP⁺ hearts were identified under fluorescent light and collected in fresh EDM. These hearts were further pooled in a 1.5 ml microfuge tube, pelleted and the preparations were stored at -80 °C after removing the media. A pool of 30 extracted hearts was used for RNA extraction.

RT-qPCR. RNA from adult heart ventricles and 48 hpf embryos was extracted using Trizol. RNA from extracted larval hearts and LMD samples was extracted using miRNeasy Micro Kit (Qiagen), and the cDNA prepared (Maxima First Strand cDNA Synthesis Kit for RT-qPCR, Thermo Fisher Scientific) was used to perform RT-qPCR (CFX Connect Real-Time System, Biorad). The primers used for RT-qPCR are listed in Supplementary Table 2. *rpl13* was used as an internal control. The Ct values of the genes in the control samples are listed in Supplementary Table 3.

Generation of mutants and transgenic zebrafish. *inhbaa* and *mstnb* mutants were generated using TALEN-induced mutagenesis. The TALENs were designed and cloned according to Golden Gate Assembly⁶⁶. The TALEN arms targeting *inhbaa* had the following RVDs: NN NG NN NN NG NN NN NI NN NN HD NI NN NG NN and NN HD NI NN NN NG NN HD NI NN HD NI NG NN NG. The TALEN arms targeting *mstnb* had the following RVDs: NN NN NI NN NI NG NI NG NI NI HD NN NN HD NN HD and HD NN HD NN NG NG HD HD NG HD HD NN NG NN NN HD. The TALEN mRNA were injected in one-cell stage embryos and mutant alleles, *mstnb^{bms5}* and *inhbaa^{bms37}* were recovered by performing High Resolution Melt Analysis, using the following primers: *inhbaa_F-5'-AGAGCGAGGACGAGGGAG-3'*, *inhbaa_R-5'-GTGTGTGATGTTGGGTCGCT-3'* and *mstnb_F-5'-GTGTATTAATTCATGTGGTCCAG-3'*, *mstnb_R-5'-GAACACTGCTCGTTCTCCTC-3'*. The F1 heterozygous animals were intercrossed to raise F2 adults, which were used in the experiments.

For generating OE transgenes under the control of *myl7* promoter, the CDS of *mstnb* and *inhbaa* was PCR amplified and fused with a self-cleaving peptide 2A and H2B-EGFP, using Cold Fusion technology (System Biosciences, CA, USA). A total of 18 pg of each of these constructs were co-injected with 20 pg Tol2 mRNA into one-cell stage embryos. The transgenic fish obtained were named as *Tg(myl7:mstnb-2A-H2B-EGFP)bnsl45* and *Tg(myl7:inhbaa-2A-H2B-EGFP)bnsl46*. The founders were outcrossed with *Tg(-0.8myl7:nlDsRedExpress)hsc4* to generate stable lines, which were used in the experiments.

mRNA overexpression. Full length *mstnb* and *inhbaa* CDS was amplified from cDNA and cloned into pcDNA3.1. *myl7:mstnb-2A-H2B-mcherry* and *myl7:inhbaa-2A-H2B-mcherry* constructs were generated using Cold Fusion technology. For mRNA synthesis, *mstnb-2A-H2B-mcherry* and *inhbaa-2A-H2B-mcherry* CDS was cloned into pcDNA3.1. mRNA was synthesized using the mMESAGE mMACHINE kit and 100 pg of each mRNA was injected into *Tg(ARE:EGFP)* and *Tg(12XSBE:EGFP)* embryos at one-cell stage.

Generation of constitutively active constructs. Constitutively active versions of Smad2, Smad3a, and Smad3b were generated by site-directed mutagenesis of their C-terminal serines to aspartic acids in the SSXS phosphorylation motifs (phosphomimetic mutation)⁶⁷. By using Cold Fusion technology, these constitutively active versions were cloned into a Tol2 vector under the control of *myl7* promoter, *Tg(myl7:H2B-EGFP-2A-caSmad2)*, *Tg(myl7:H2B-EGFP-2A-caSmad3a)*, *Tg(myl7:H2B-EGFP-2A-caSmad3b)*. Similarly, *Tg(myl7:H2B-EGFP)* was generated as control. 20 pg of each of these constructs were co-injected with 20 pg Tol2 mRNA into one-cell stage embryos.

Morpholinos. The following MOs were purchased from GeneTools (Philomath, OR) and injected at the one-cell stage at the indicated amounts in all experiments described: *acvr2aa* ATG MO—1.5 ng (5'-CCAGCTTTGTTGCAGGTCCCATTTTT-3'), *acvr2ab* splice MO—2 ng (5'-TGGCTGCACAAACACAGATTAAT-3'), *acvr2ba* ATG MO—1 ng (5'-TGAGCAGAAAGCGAACATATTCCT-3'), *acvr2bb* ATG MO—0.5 ng (5'-AGCCAGCAGGAAACAAACATATTC-3') and control MO—concentrations similar to experimental MOs (5'-CCTCTTACCT-CAGTTACAATTTATA-3'). All doses were determined as optimal by titration (no toxic effects were observed).

Histology and in situ hybridization. The hearts were fixed in 4% paraformaldehyde (PFA) and 7 μ m thick paraffin sections or 12 μ m thick cryosections were obtained. For H&E staining, the cryosections were stained with acidic hemalum (Waldeck) for 10 min, washed in running tap water for 2 min and rinsed in deionized water. Further, the sections were stained with eosin (Waldeck) for 6 min, dehydrated in 100% ethanol, cleared in xylene and mounted in entellan (Merck).

For AFOG staining, paraffin sections were fixed with Bouin's solution overnight at room temperature (RT) and stained according to the manufacturer's instructions (Genovva), without hematoxylin solution. To perform in situ hybridization⁶⁸, cryosections were permeabilized in 5 $\mu\text{g ml}^{-1}$ proteinase K (Roche) for 15 min at RT, followed by acetylation for 2 min and pre-incubation in hybridization buffer for 3 h at 70 °C. Later, the sections were incubated with DIG-labeled RNA antisense probes overnight at 70 °C. Next, the sections were washed and incubated with alkaline phosphatase-conjugated anti-digoxigenin antibody (Roche) overnight at 4 °C. Finally, after washing, the signal was detected with NBT-BCIP staining solution (Roche). Probes for in situ hybridization were generated by using the following primer sequences: *mstnb_insitu_F-5'-CCCATGTTC AAGTAGATCGG-3'*, *mstnb_insitu_R-5'-ATTGTCCATTCCCGAGTCCA-3'*, *inhbaa_insitu_F-5'-ATC ATCAGT TCGCTGAAACC-3'* and *inhbaa_insitu_R-5'-GAGAGTTCGCTTG AGGCAG-3'*.

Immunofluorescence. To perform immunofluorescence⁷, cryosections were fixed in 4% PFA for 15 min, followed by antigen retrieval for 20 min at 95 °C (for PCNA antibody staining), permeabilization in 0.5% Triton-X for 15 min at RT and incubation in blocking buffer (1% BSA in PBS) for 1 h at RT. Later, the sections were incubated in primary antibody overnight at 4 °C. Next, after washing, the sections were incubated with secondary antibody overnight at 4 °C. Finally, the immunostained slides were mounted with mowiol for imaging. To perform immunofluorescence⁶⁹, whole-mount larvae were fixed in 4% PFA overnight at 4 °C, followed by incubation in permeabilization solution (0.3% Triton-X, 1% DMSO, 1% BSA, and 0.1% Tween-20) for 3 h at RT. Further, the larvae were incubated in blocking solution (1% DMSO, 2% FBS, 1% BSA, and 0.1% Tween-20) for 1 h at RT. Next, the larvae were incubated in primary antibody overnight at 4 °C. Later, after washing, the larvae were incubated in secondary antibody overnight at 4 °C. Finally, the stained larvae were washed, mounted in 1.5% low melting agarose for imaging. Primary antibodies used for immunofluorescence were anti-PCNA at 1:200 (mouse; Dako), anti-DsRed at 1:300 (rabbit, Clontech), anti-pSmad3 at 1:200 (rabbit; Abcam), anti-MF-20 at 1:500 (mouse; eBioscience), anti-GFP at 1:500 (chicken, Aves Labs) and anti-N2.261 at 1:50 (mouse, H.M. Blau, Developmental Studies Hybridoma Bank). Secondary antibodies were used at 1:500 (Life Technologies).

Imaging and quantification. The immunostained slides and larvae were imaged at $\times 20$ magnification and $\times 40$ magnification, respectively using LSM700/LSM800 confocal microscopes (Zeiss). After imaging, the acquired confocal z-stacks were processed and cell counting was performed with ZEN (Zeiss), Fiji, and Imapris (Bitplane) softwares. Bright field images were obtained with stereomicroscopes (SMZ25, Nikon and Stereodiscovery V8, Zeiss). Ventricular, atrial and eye sizes were measured by using ZEN software (apex to base). Ventricular wall thickness was also measured by using ZEN software, by taking the average of three regions near the apex.

Genotyping. For genotyping the immunostained larvae obtained by crossing different transgenic backgrounds, PCR was performed on genomic DNA using the primers listed in Supplementary Table 4. *erbb2^{st61}* mutants were genotyped⁶³ by using PCR-based restriction fragment length polymorphism analysis. PCR products obtained from genomic DNA samples (using primer pairs listed in Supplementary Table 4) were cut with BsrGI, resulting in a genotype-specific DNA band pattern.

EdU treatment. For EdU incorporation analysis, adult fish were anaesthetized with 0.016% tricaine and 200 μg of EdU (Invitrogen) was injected intraperitoneally. The hearts were sampled after 3 days of EdU incubation and fixed in 4% PFA. 1 mM EdU was used to incubate embryos from 48 hpf to 72 hpf and larvae from 96 hpf to 120 hpf, followed by fixation in 4% PFA. EdU labeling was performed according to the manufacturer's protocol (Invitrogen).

ErBb2 and TGF- β signaling inhibitor treatments. The ErBb2 signaling inhibitor (PD168393, Calbiochem)⁷⁰, Smad3 phosphorylation inhibitor (SIS3, Calbiochem)⁵⁰ and Activin type 1 receptor inhibitor (SB431542, Calbiochem)⁵² were used to treat the embryos or larvae. The embryos were treated with 3 μM SIS3 and 10 μM SB431542 from 36 hpf to 72 hpf. The larvae were treated with 10 μM PD168393 and 3 μM SIS3 from 84 hpf to 120 hpf. All inhibitors were dissolved in DMSO and added to egg water. Control fish were incubated in 1% DMSO in egg water.

Statistical analysis. No statistical methods were used to predetermine sample size. The experiments were not randomized. The investigators were not blinded to allocation during experiments or outcome assessment, except for the data shown in Fig. 4e–s. GraphPad software was used to perform statistical analysis. Data are represented as mean \pm s.e.m. *P*-values were calculated by two-tailed Student's *t* test.

Data availability. The authors declare that all data supporting the findings of this study are available within the article and its Supplementary Information files or from the corresponding author upon reasonable request. Microarray raw and normalized data have been deposited in the NCBI-GEO database under the accession code: GSE89259.

Received: 10 March 2017 Accepted: 27 October 2017

Published online: 01 December 2017

References

- Steinhauser, M. L. & Lee, R. T. Regeneration of the heart. *EMBO Mol. Med.* **3**, 701–712 (2011).
- Mozaffarian, D. et al. Heart Disease and Stroke Statistics-2016 Update: a report from the American Heart Association. *Circulation* **133**, e38–e360 (2016).
- Chong, J. J. et al. Human embryonic-stem-cell-derived cardiomyocytes regenerate non-human primate hearts. *Nature* **510**, 273–277 (2014).
- Bersell, K., Arab, S., Haring, B. & Kühn, B. Neuregulin1/ErbB4 signaling induces cardiomyocyte proliferation and repair of heart injury. *Cell* **138**, 257–270 (2009).
- Qian, L. et al. In vivo reprogramming of murine cardiac fibroblasts into induced cardiomyocytes. *Nature* **485**, 593–598 (2012).
- Poss, K. D., Wilson, L. G. & Keating, M. T. Heart regeneration in zebrafish. *Science* **298**, 2188–2190 (2002).
- Chablais, F., Veit, J., Rainer, G. & Jazwińska, A. The zebrafish heart regenerates after cryoinjury-induced myocardial infarction. *BMC Dev. Biol.* **11**, 21 (2011).
- Wang, J. et al. The regenerative capacity of zebrafish reverses cardiac failure caused by genetic cardiomyocyte depletion. *Development* **138**, 3421–3430 (2011).
- Jopling, C. et al. Zebrafish heart regeneration occurs by cardiomyocyte dedifferentiation and proliferation. *Nature* **464**, 606–609 (2010).
- Kikuchi, K. et al. Primary contribution to zebrafish heart regeneration by gata4 (+) cardiomyocytes. *Nature* **464**, 601–605 (2010).
- Wu, C.-C. C. et al. Spatially resolved genome-wide transcriptional profiling identifies BMP signaling as essential regulator of zebrafish cardiomyocyte regeneration. *Dev. Cell* **36**, 36–49 (2016).
- Kikuchi, K. Advances in understanding the mechanism of zebrafish heart regeneration. *Stem Cell Res.* **13**, 542–555 (2014).
- Marín-Juez, R. et al. Fast revascularization of the injured area is essential to support zebrafish heart regeneration. *Proc. Natl Acad. Sci. USA* **113**, 11237–11242 (2016).
- Gemberling, M., Karra, R., Dickson, A. L. & Poss, K. D. Nrg1 is an injury-induced cardiomyocyte mitogen for the endogenous heart regeneration program in zebrafish. *Elife* **1**, 4 (2015).
- D'Uva, G. et al. ERBB2 triggers mammalian heart regeneration by promoting cardiomyocyte dedifferentiation and proliferation. *Nat. Cell Biol.* **17**, 627–638 (2015).
- Liu, J. et al. A dual role for ErbB2 signaling in cardiac trabeculation. *Development* **137**, 3867–3875 (2010).
- Rasouli, S. J. & Stainier, D. Y. Regulation of cardiomyocyte behavior in zebrafish trabeculation by Neuregulin 2a signaling. *Nat. Commun.* **8**, 15281 (2017).
- Polizzotti, B. D. et al. Neuregulin stimulation of cardiomyocyte regeneration in mice and human myocardium reveals a therapeutic window. *Sci. Transl. Med.* **7**, 281ra45 (2015).
- Ahuja, S., Dogra, D., Stainier, D. Y. & Reischauer, S. Id4 functions downstream of Bmp signaling to restrict TCF function in endocardial cells during atrioventricular valve development. *Dev. Biol.* **412**, 71–82 (2016).
- Siegel, P. M. & Massagué, J. Cytostatic and apoptotic actions of TGF- β in homeostasis and cancer. *Nat. Rev. Cancer* **3**, 807–821 (2003).
- Massagué, J. & Gomis, R. R. The logic of TGF β signaling. *FEBS Lett.* **580**, 2811–2820 (2006).
- Massagué, J. TGF β signalling in context. *Nat. Rev. Mol. Cell Biol.* **13**, 616–630 (2012).
- Sartori, R., Gregorevic, P. & Sandri, M. TGF β and BMP signaling in skeletal muscle: potential significance for muscle-related disease. *Trends Endocrinol. Metab.* **25**, 464–471 (2014).
- Derynck, R. & Zhang, Y. E. Smad-dependent and Smad-independent pathways in TGF- β family signalling. *Nature* **425**, 577–584 (2003).
- Castillero, E. et al. Cardiac myostatin upregulation occurs immediately after myocardial ischemia and is involved in skeletal muscle activation of atrophy. *Biochem. Biophys. Res. Commun.* **457**, 106–111 (2015).
- Yndestad, A. et al. Elevated levels of activin A in heart failure: potential role in myocardial remodeling. *Circulation* **109**, 1379–1385 (2004).
- Li, R. K. et al. Overexpression of transforming growth factor- β 1 and insulin-like growth factor-I in patients with idiopathic hypertrophic cardiomyopathy. *Circulation* **96**, 874–881 (1997).
- Euler-Taimor, G. & Heger, J. The complex pattern of SMAD signaling in the cardiovascular system. *Cardiovasc. Res.* **69**, 15–25 (2006).
- Zeisberg, E. M. et al. Endothelial-to-mesenchymal transition contributes to cardiac fibrosis. *Nat. Med.* **13**, 952–961 (2007).

30. Koitabashi, N. et al. Pivotal role of cardiomyocyte TGF- β signaling in the murine pathological response to sustained pressure overload. *J. Clin. Invest.* **121**, 2301–2312 (2011).
31. Chablais, F. & Jazwinska, A. The regenerative capacity of the zebrafish heart is dependent on TGF β signaling. *Development* **139**, 1921–1930 (2012).
32. Whittemore, L.-A. A. et al. Inhibition of myostatin in adult mice increases skeletal muscle mass and strength. *Biochem. Biophys. Res. Commun.* **300**, 965–971 (2003).
33. Haidet, A. M. et al. Long-term enhancement of skeletal muscle mass and strength by single gene administration of myostatin inhibitors. *Proc. Natl Acad. Sci. USA* **105**, 4318–4322 (2008).
34. Biesemann, N. et al. Myostatin regulates energy homeostasis in the heart and prevents heart failure. *Circ. Res.* **115**, 296–310 (2014).
35. Rodgers, B. D. et al. Myostatin represses physiological hypertrophy of the heart and excitation-contraction coupling. *J. Physiol.* **587**, 4873–4886 (2009).
36. Wagner, K. R., Liu, X., Chang, X. & Allen, R. E. Muscle regeneration in the prolonged absence of myostatin. *Proc. Natl Acad. Sci. USA* **102**, 2519–2524 (2005).
37. Latres, E. et al. Myostatin blockade with a fully human monoclonal antibody induces muscle hypertrophy and reverses muscle atrophy in young and aged mice. *Skelet Muscle* **5**, 34 (2015).
38. Jaźwińska, A., Badakov, R. & Keating, M. T. Activin- β A signaling is required for zebrafish fin regeneration. *Curr. Biol.* **17**, 1390–1395 (2007).
39. Biesemann, N. et al. Myostatin induces interstitial fibrosis in the heart via TAK1 and p38. *Cell Tissue Res.* **361**, 779–787 (2015).
40. Sallin, P., Preux Charles, A.-S. S., de Duruz, V., Pfefferli, C. & Jaźwińska, A. A dual epimorphic and compensatory mode of heart regeneration in zebrafish. *Dev. Biol.* **399**, 27–40 (2015).
41. Rebbapragada, A., Benchabane, H., Wrana, J. L., Celeste, A. J. & Attisano, L. Myostatin signals through a transforming growth factor beta-like signaling pathway to block adipogenesis. *Mol. Cell Biol.* **23**, 7230–7242 (2003).
42. Chen, X., Weisberg, E., Fridmacher, V. & Watanabe, M. Smad4 and FAST-1 in the assembly of activin-responsive factor. *Nature* **389**, 85–89 (1997).
43. Chen, X., Rubock, M. J. & Whitman, M. A transcriptional partner for MAD proteins in TGF-beta signalling. *Nature* **383**, 691–696 (1996).
44. Labbé, E., Silvestri, C., Hoodless, P. A., Wrana, J. L. & Attisano, L. Smad2 and Smad3 positively and negatively regulate TGF beta-dependent transcription through the forkhead DNA-binding protein FAST2. *Mol. Cell* **2**, 109–120 (1998).
45. Jonk, L., Itoh, S., Heldin, C.-H., Dijke, Pten. & Kruijer, W. Identification and functional characterization of a smad binding element (SBE) in the JunB promoter that acts as a transforming growth factor- β , activin, and bone morphogenetic protein-inducible Enhancer. *J. Biol. Chem.* **273**, 21145–21152 (1998).
46. Stroschein, S. L., Wang, W. & Luo, K. Cooperative binding of Smad proteins to two adjacent DNA elements in the plasminogen activator inhibitor-1 promoter mediates transforming growth factor beta-induced smad-dependent transcriptional activation. *J. Biol. Chem.* **274**, 9431–9441 (1999).
47. Boxtel, A. Lvan. et al. A temporal window for signal activation dictates the dimensions of a nodal signaling domain. *Dev. Cell* **35**, 175–185 (2015).
48. Casari, A. et al. A Smad3 transgenic reporter reveals TGF-beta control of zebrafish spinal cord development. *Dev. Biol.* **396**, 81–93 (2014).
49. Choi, W.-Y. Y. et al. In vivo monitoring of cardiomyocyte proliferation to identify chemical modifiers of heart regeneration. *Development* **140**, 660–666 (2013).
50. Jinnin, M., Ihn, H. & Tamaki, K. Characterization of SIS3, a novel specific inhibitor of Smad3, and its effect on transforming growth factor-beta1-induced extracellular matrix expression. *Mol. Pharmacol.* **69**, 597–607 (2006).
51. Denis, J.-F. F. et al. Activation of Smad2 but not Smad3 is required to mediate TGF- β signaling during axolotl limb regeneration. *Development* **143**, 3481–3490 (2016).
52. Inman, G. J. et al. SB-431542 is a potent and specific inhibitor of transforming growth factor-beta superfamily type I activin receptor-like kinase (ALK) receptors ALK4, ALK5, and ALK7. *Mol. Pharmacol.* **62**, 65–74 (2002).
53. Lee, S. J. & McPherron, A. C. Regulation of myostatin activity and muscle growth. *Proc. Natl Acad. Sci. USA* **98**, 9306–9311 (2001).
54. Ho, D. M. & Whitman, M. TGF-beta signaling is required for multiple processes during Xenopus tail regeneration. *Dev. Biol.* **315**, 203–216 (2008).
55. Thenappan, A. et al. Role of transforming growth factor beta signaling and expansion of progenitor cells in regenerating liver. *Hepatology* **51**, 1373–1382 (2010).
56. Chen, H. et al. Analysis of ventricular hypertrabeculation and noncompaction using genetically engineered mouse models. *Pediatr. Cardiol.* **30**, 626–634 (2009).
57. Wang, T. et al. The immunophilin FKBP12 functions as a common inhibitor of the TGF beta family type I receptors. *Cell* **86**, 435–444 (1996).
58. Kretzschmar, M., Doody, J., Timokhina, I. & Massagué, J. A mechanism of repression of TGFbeta/Smad signaling by oncogenic Ras. *Genes Dev.* **13**, 804–816 (1999).
59. Zhou, P. & Pu, W. T. Recounting cardiac cellular composition. *Circ. Res.* **118**, 368–370 (2016).
60. Brown, K. A., Pietenpol, J. A. & Moses, H. L. A tale of two proteins: differential roles and regulation of Smad2 and Smad3 in TGF-beta signaling. *J. Cell Biochem.* **101**, 9–33 (2007).
61. Petersen, M. et al. Smad2 and Smad3 have opposing roles in breast cancer bone metastasis by differentially affecting tumor angiogenesis. *Oncogene* **29**, 1351–1361 (2010).
62. Míguez, D. G., Gil-Guiñón, E., Pons, S. & Martí, E. Smad2 and Smad3 cooperate and antagonize simultaneously in vertebrate neurogenesis. *J. Cell Sci.* **126**, 5335–5343 (2013).
63. Lyons, D. A. et al. *erbb3* and *erbb2* are essential for schwann cell migration and myelination in zebrafish. *Curr. Biol.* **15**, 513–524 (2005).
64. Takeuchi, J. K. et al. Chromatin remodelling complex dosage modulates transcription factor function in heart development. *Nat. Commun.* **2**, 187 (2011).
65. Burns, G. C. & MacRae, C. A. Purification of hearts from zebrafish embryos. *Biotechniques* **40**, 274 (2006).
66. Cermak, T. et al. Efficient design and assembly of custom TALEN and other TAL effector-based constructs for DNA targeting. *Nucleic Acids Res.* **39**, e82 (2011).
67. Chipuk, J. E. et al. The androgen receptor represses transforming growth factor-beta signaling through interaction with Smad3. *J. Biol. Chem.* **277**, 1240–1248 (2002).
68. Bae, Y.-K. K. et al. Anatomy of zebrafish cerebellum and screen for mutations affecting its development. *Dev. Biol.* **330**, 406–426 (2009).
69. Beis, D. et al. Genetic and cellular analyses of zebrafish atrioventricular cushion and valve development. *Development* **132**, 4193–4204 (2005).
70. Reischauer, S., Arnaout, R., Ramadass, R. & Stainier, D. Y. Actin binding GFP allows 4D in vivo imaging of myofilament dynamics in the zebrafish heart and the identification of *Erb2* signaling as a remodeling factor of myofibril architecture. *Circ. Res.* **115**, 845–856 (2014).

Acknowledgements

We would like to thank Veronica Uribe Sokolov, Anoop V. Cherian, Vanesa Jiménez Amilburu, Michele Marass, Jason Kuan Han Lai, and Raoul F.V. Germano for helpful discussions, Chi-Chung Wu, Rubén Marín-Juez, Arica Beisaw, and Alethia Villasenor for comments on the manuscript, Srinivas Allanki for help with statistics, Radhan Ramadass for microscopy guidance, Beate Grohmann for help with cryosectioning, Anabela Ben-simon Brito for help with LMD, Hans-Martin Maischein for help with injections, and Rita Retzlöff and Martin Laszczyk for zebrafish care. This work was supported by fellowships from the IMPRS-HLR (D.D.), the DFG RE3148/1-1 and SFB 1213, project B1 (S.R.) and grants from the NIH (HL54737), the Packard Foundation, the Leducq Foundation and the Max Planck Society (D.Y.R.S.).

Author contributions

D.D. designed the study, performed the experiments, analyzed the data and wrote the manuscript; S.A. performed parts of the histology experiments; H.-T.K. performed in situ hybridization experiments; S.J.R. provided an unpublished reagent; D.Y.R.S. and S.R. designed the study, analyzed the data, wrote the manuscript and supervised the work. All the authors commented on the manuscript.

Additional information

Supplementary Information accompanies this paper at doi:10.1038/s41467-017-01950-1.

Competing interests: The authors declare no competing financial interests.

Reprints and permission information is available online at <http://npg.nature.com/reprintsandpermissions/>

Publisher's note: Springer Nature remains neutral with regard to jurisdictional claims in published maps and institutional affiliations.

 **Open Access** This article is licensed under a Creative Commons Attribution 4.0 International License, which permits use, sharing, adaptation, distribution and reproduction in any medium or format, as long as you give appropriate credit to the original author(s) and the source, provide a link to the Creative Commons license, and indicate if changes were made. The images or other third party material in this article are included in the article's Creative Commons license, unless indicated otherwise in a credit line to the material. If material is not included in the article's Creative Commons license and your intended use is not permitted by statutory regulation or exceeds the permitted use, you will need to obtain permission directly from the copyright holder. To view a copy of this license, visit <http://creativecommons.org/licenses/by/4.0/>.

© The Author(s) 2017